IPP-Report

Max-Planck-Institut
für Plasmaphysik

Ya. Kolesnichenko, V. V. Lutsenko, H. Wobig,
Yu. V. Yakovenko, O. P. Fesenyuk

Alfvén Eigenmodes in Helias Configurations (Part I)

IPP III/261

Mai 2000

Ya. Kolesnichenko, V. V. Lutsenko, H. Wobig,
Yu. V. Yakovenko, O. P. Fesenyuk

Alfvén Eigenmodes in Helias Configurations (Part I)

IPP III/261
Mai 2000

Alfvén eigenmodes in Helias configurations (part I)

Ya.I. Kolesnichenko*, V.V. Lutsenko*, H. Wobig**,

Yu.V. Yakovenko*, and O.P. Fesenyuk*

*Scientific Centre "Institute for Nuclear Research", 03680 Kyiv, Ukraine

**Max-Planck Institut für Plasmaphysik, IPP-EURATOM Association,

D-85748 Garching bei München, Germany

(May 10, 2000)

Abstract

An equation of shear Alfvén eigenmodes (AE) for Helias configurations is derived. The metric tensor coefficients, which are contained in this equation, are calculated analytically. Two numerical codes are developed: the first one, COBRA (COntinuum BRAnches), is intended for the investigation of the structure of Alfvén continuum; the second, BOA (Branches Of Alfvén modes), solves the eigenvalue problem. The family of possible gaps in Alfvén continuum of a Helias configuration is obtained. It is predicted that there exist gaps which arise due to or are strongly affected by the variation of the shape of the plasma cross section along the large azimuth of the torus. In such gaps, discrete eigenmodes, namely, helicity-induced eigenmodes (HAE_{21}) and mirror-induced eigenmodes (MAE) are found. It is shown that the combined action of the weak magnetic shear and the low plasma density at the edge may suppress the AEs with a wide region of localization. In addition to AEs residing in the continuum gaps, global AEs (GAE) are studied.

I. INTRODUCTION

It is known that shear Alfvén waves are weakly damped in low-β Maxwellian plasma (β is the ratio of the plasma pressure to the magnetic field pressure) and, therefore, can be destabilized in the presence of a rather small population of energetic ions, in particular, fusion-produced alpha particles. An Alfvén instability of a fusion plasma caused by alpha particles was first studied by Belikov, Kolesnichenko and Oraevskij as long ago as 1968 [1]. The instability considered in Ref. [1] was associated with the non-equilibrium velocity distribution of alphas. Later, in 1975, Mikhailovskij has considered an Alfvén instability induced by the spatial inhomogeneity of alpha particle distribution [2]. Both mentioned works were based on the local approach, which enabled to evaluate the growth rate of the instabilities. However, the local approach is not sufficient because it does not give an answer to the question what is the spatial structure of the modes and does not allow to take into account all mechanisms of the wave damping involved; furthermore, it is not clear from the local analysis whether a mode exists at all in a real inhomogeneous plasma. Thus, a solution of an eigenvalue problem is required for reliable predictions. The study of Alfvén instabilities with employing the eigenmode analysis was started by Rosenbluth and Rutherford in 1975 [3]. Research in this way resulted in the prediction of the instability of global Alfvén eigenmodes (GAE) in tokamaks [4,5] and a number of other instabilities where destabilized modes were associated with the break of the poloidal symmetry of the magnetic configuration. In particular, the instabilities of toroidicity-induced Alfvén eigenmodes (TAE) [6], ellipticity-induced and noncircular triangularity-induced Alfvén eigenmodes (EAE and NAE) [7] were predicted. The mentioned eigenmodes have frequencies that do not intersect the Alfvén continuous spectrum (which is determined by the equation $\omega = \omega_A(r) \equiv |k_\parallel(r)| v_A(r)$ with $k_\parallel$ the longitudinal wave number, v_A the Alfvén velocity, and r the flux surface radius), i.e., lie either in gaps of the continuum or below the continuum, which minimizes their damping. The existence of the gaps for TAE modes was shown earlier in Ref. [8], and for EAE modes, in Ref. [9]. An additional gap containing beta-induced eigenmodes (BAE) is associated with finite β and arises due

to coupling at low frequencies between shear Alfvén modes and compressible acoustic waves [10,11]. Taking into account the effects of non-ideal MHD (finite Larmor radius, finite electron mass correction, viscosity) resulted in the discovery of kinetic Alfvén waves with the local frequencies determined by the Alfvén continuum (KAE) [12], which can be coupled due to toroidicity, producing kinetic toroidal eigenmodes (KTAE) [13] with the frequencies inside the Alfvén continuum (just above the top edge of the TAE gap). When the energy content of the energetic particles is comparable to that of the bulk plasma, energetic particle continuum modes (EPM) [14] also known as resonant toroidal Alfvén modes (RTAE) [15] can arise, with the frequencies being determined by the energetic particles and close to their transit, bounce and precession frequencies. It was found that destabilized AEs can result in severe loss of alpha particles even when the amplitudes of the perturbed magnetic field are very low, being about 5×10^{-4} of the equilibrium magnetic field [16,17].

These theoretical predictions stimulated the experimental study of Alfvén instabilities. Experiments on tokamaks have shown that the destabilization of Alfvén eigenmodes (AE) may result in the loss of a considerable fraction of energetic ions (see, e.g., an overview [18]), which, in turn, has led to further development of the theory, including nonlinear studies, and codes for numerical simulations.

Alfvén instabilities in stellarator plasmas were also investigated both experimentally and theoretically, see, e.g., Refs. [19–23]. However, they are studied much less than those in tokamaks in spite of the fact that there must exist more variety of AE modes in the helical devices because the symmetry of the magnetic configuration in these systems is broken in both poloidal and toroidal directions.

Nowadays, AE modes are a subject of extensive studies (see, e.g., a recent conference report [24]).

The purpose of this work is to investigate the shear Alfvén spectrum and the spatial structure of AEs in Helias (HELIcal Advanced Stellarator) configurations of Wendelstein line, first of all, in a Helias reactor [25–27]. A related problem was addressed in recent publications by C. Nührenberg [28,29], where eigenmodes in the stellarators Wendelstein

7-X (W7-X) [30,26] and Wendelstein 7-AS (W7-AS) [31] were studied. In Refs. [28,29] the analysis was based on the use of the CAS3D3 stability code [32,28]. In particular, it was found in Ref. [28] that in the W7-X high-ι high-mirror variant, which has many similar features with the Helias reactor, there exist spectral gaps and gap modes in Alfvén and sound continuum branches, exhibiting strong interaction of sound and Alfvén branches in the lower part of the stable spectrum (note that in Ref. [28] the plasma density was assumed to be homogeneous). In the present work we employ another approach, deriving an equation which describes only shear Alfvén modes (in contrast to Refs. [28,29], which treat the full ideal MHD equations) and then use the metric tensor coefficients found analytically. The procedure of numerical investigation of AEs with the use of our equations is much simpler and less time-consuming than that of Refs. [28,29]. On the other hand, one can expect that the results based on the derived equations are sufficiently exact to predict features of AE modes, at least, in the high-frequency part of the spectrum, where the effect of the sound spectrum is negligible.

The structure of the work is the following. In Sec. II, a basic equation for the shear AE modes is derived in flux coordinates in the framework of ideal MHD. In Sec III, possible gaps in the Alfvén continuum and corresponding kinds of AEs are studied, and their characteristic frequencies are determined. The width of the gaps in the approximation of weak mode coupling is analyzed in Sec. IV. Also, the effect of multiple wave interaction on the gaps is studied perturbatively in this section. In Sec. V the general pattern of the Alfvén continuum in a Helias is studied numerically without using the assumption that the coupling parameter is small. Equations for AEs, which describe helicity-induced and mirror-induced AEs, are solved numerically in Sec. VI. In Sec. VII, GAE modes are considered. Sec. VIII summarizes the obtained results and contains conclusions following from the work. In Appendix A, the metric tensor components used in our studies of AEs are calculated. Appendix B contains the substantiation of the equation of the Alfvén continuum, on which the calculation in Sec. V is based.

This work represents the first part of the authors' investigation of the frequency spectrum and the structure of the AE modes.

II. BASIC EQUATION FOR SHEAR ALFVÉN EIGENMODES IN HELIAS CONFIGURATIONS

In order to derive an equation describing AEs, we proceed from the equation $\nabla \cdot \vec{\tilde{j}} = 0$, where $\vec{\tilde{j}}$ is the plasma current density associated with the Alfvén perturbations. This equation can be written as follows:

$$\nabla \cdot (\tilde{j}_{\parallel} \vec{b}) + \nabla \cdot \vec{\tilde{j}}_{\perp} = 0, \tag{1}$$

where $\vec{b} = \vec{B}_0 / B_0$, $\vec{B}$ is the magnetic field; the subscript "0" refers to equilibrium quantities, whereas tilde refers to perturbed quantities; the subscripts $\perp$ and $\parallel$ label the vector components that are perpendicular and parallel to $\vec{B}_0$, respectively. Using the ideal MHD approximation, we assume the longitudinal component of the perturbed electric field to vanish, $\tilde{E}_{\parallel} = 0$. In addition, as we are interested in shear Alfvén waves, we take $\tilde{B}_{\parallel} = 0$. This enables us to express the perturbed electromagnetic field through the electric potential as follows (we suppose that the perturbed quantities vary in time as $\exp(-i\omega t)$ and take $\vec{\tilde{A}}_{\perp} = 0$):

$$\vec{\tilde{E}} = -\nabla_{\perp} \tilde{\Phi}, \qquad \vec{\tilde{B}} = \nabla \times \tilde{A} \vec{b}, \tag{2}$$

where

$$\tilde{A} = \frac{c}{i\omega} \nabla_{\parallel} \tilde{\Phi}, \tag{3}$$

$\nabla_{\perp} = \nabla - \vec{b} \nabla_{\parallel}$, $\nabla_{\parallel} = \vec{b} \cdot \nabla$, $\tilde{A}$ is the longitudinal component of the vector potential (the subscript $\parallel$ is omitted).

Now we find the perturbed currents, $\tilde{j}_{\parallel}$ and $\vec{\tilde{j}}_{\perp}$, in terms of $\tilde{\Phi}$. Using the equation $\nabla \times \vec{B} = 4\pi \vec{j}/c$, we obtain:

$$\frac{4\pi}{c} \tilde{j}_{\parallel} = \frac{1}{B_0} \nabla \cdot \left(\tilde{A} B_0 \vec{\mathcal{K}} - B_0 \nabla_{\perp} \tilde{A} \right) + \frac{\vec{\tilde{B}}}{B_0} \frac{4\pi}{c} \vec{j}_{0\perp}, \tag{4}$$

where $\vec{\mathcal{K}} = (\vec{b} \cdot \nabla) \vec{b} = |B_0|^{-2} \nabla_{\perp} (B_0^2/2 + 4\pi p_0)$ is the magnetic field line curvature, p is the plasma pressure. In order to find the perpendicular current, we proceed from a linearized

equation of the plasma motion in the ideal MHD, where we neglect the perturbed plasma pressure. Assuming that the equilibrium velocity of the plasma motion vanishes, we write this equation as follows:

$$-i\omega c\rho_0 \vec{\tilde{u}} = \vec{j}_0 \times \vec{\tilde{B}} + \vec{\tilde{j}} \times \vec{B}_0, \tag{5}$$

where ρ is the mass density. Then, using the Ohm law, $\vec{E} + \vec{u} \times \vec{B}/c = 0$, we find:

$$\vec{\tilde{j}}_\perp = \frac{i\omega c^2}{4\pi v_A^2} \nabla_\perp \Phi + j_{0\parallel} \frac{\vec{\tilde{B}}}{B_0}, \tag{6}$$

where $v_A = B_0/\sqrt{4\pi\rho_0}$. Substituting Eqs. (4)–(6) to Eq. (1), we obtain:

$$B_0 \nabla_\parallel \frac{1}{|B_0|^2} \left[\nabla \cdot \left(\tilde{A} B_0 \vec{\mathcal{K}} - B_0 \nabla_\perp \tilde{A} \right) + \frac{4\pi}{c} \vec{j}_{0\perp} \cdot \vec{\tilde{B}} \right]$$
$$+ i\omega \nabla \cdot \left(\frac{c}{v_A^2} \nabla_\perp \tilde{\Phi} \right) + \frac{4\pi}{c} \vec{\tilde{B}} \cdot \nabla_\perp \frac{j_{0\parallel}}{B_0} = 0. \tag{7}$$

Note that the eigenfrequencies of Eq. (7) are real. To demonstrate this, we will consider the case of vanishing equilibrium currents (which corresponds to Helias configurations). In addition, we take $p_0 = 0$, which enables us to write

$$\tilde{A} B_0 \vec{\mathcal{K}} - B_0 \nabla_\perp \tilde{A} = -|B_0|^2 \nabla_\perp \frac{\tilde{A}}{B_0}. \tag{8}$$

Then Eq. (7) is reduced to

$$\hat{M}\tilde{\Phi} + \omega^2 \hat{N}\tilde{\Phi} = 0, \tag{9}$$

where

$$\hat{M} = \nabla \cdot \left\{ \frac{\vec{b}}{B_0} \nabla \cdot \left[B_0^2 \nabla_\perp \left(\frac{\nabla_\parallel}{B_0} \right) \right] \right\}, \tag{10}$$

$$\hat{N} = \nabla \cdot \left(\frac{1}{v_A^2} \nabla_\perp \right). \tag{11}$$

The operators $\hat{M}$ and $\hat{N}$ are self-adjoint, $\hat{M}$ being positive semi-definite, and $\hat{N}$ being negative definite under fixed boundary conditions, which can be seen from the following equations:

$$\left(\tilde{\Psi}, \hat{M}\tilde{\Phi}\right) \equiv \int \tilde{\Psi}\hat{M}\tilde{\Phi}d^3x = \int B_0^2 \nabla_\perp \left(\frac{\nabla_\parallel \tilde{\Psi}}{B_0}\right) \cdot \nabla_\perp \left(\frac{\nabla_\parallel \tilde{\Phi}}{B_0}\right) d^3x, \tag{12}$$

$$\left(\tilde{\Psi}, \hat{N}\tilde{\Phi}\right) = -\int \frac{1}{v_A^2} \nabla_\perp \tilde{\Psi} \cdot \nabla_\perp \tilde{\Phi} d^3x, \tag{13}$$

where the integrals are taken over the plasma volume, $\tilde{\Psi}$ is an arbitrary function vanishing at the plasma boundary. Therefore, we can conclude that the eigenfrequencies of Eq. (9) are real:

$$\omega^2 = -\frac{(\tilde{\Phi}, \hat{M}\tilde{\Phi})}{(\tilde{\Phi}, \hat{N}\tilde{\Phi})} \geq 0. \tag{14}$$

For further treatment we have to specify the equilibrium plasma configuration. We consider a Helias configuration with the magnetic field strength given by [33]:

$$B_0 = \bar{B}\left[1 + \epsilon_m(\psi)\cos N\phi + \epsilon_h(\psi)\cos\left(\theta - N\phi\right) + \epsilon_t(\psi)\cos\theta + \epsilon_0(\psi)\right], \tag{15}$$

where ψ, θ, and ϕ are the magnetic flux coordinates [34,35] (ψ is the toroidal magnetic flux, θ and ϕ are the poloidal and toroidal angles, respectively); ϵ_m, ϵ_h, ϵ_t, and ϵ_0 are small compared to unity, $\epsilon_m > 0$, $\epsilon_0 > 0$, $\epsilon_h < 0$, $\epsilon_t < 0$; N is the number of periods of the magnetic field. The second, third, and fourth terms in Eq. (15) represent the mirror, helical, and toroidal harmonics of the magnetic field, the mirror harmonic being dominant in the plasma core. The last term in Eq. (15) is associated with the finite plasma pressure. The magnitudes and the radial profile shapes of ϵ_m, ϵ_h, ϵ_t in a plasma with finite β are a little bit different from those in vacuum [36,37].

In the magnetic flux coordinates [34,35] the contravariant and covariant representations of the equilibrium magnetic field take the form

$$\vec{B}_0 = \nabla\psi \times \nabla\theta + \iota\nabla\phi \times \nabla\psi, \tag{16}$$

$$\vec{B}_0 = B_\psi(\psi,\theta,\phi)\nabla\psi + B_\theta(\psi)\nabla\theta + B_\phi(\psi)\nabla\phi, \tag{17}$$

where B_ψ, B_θ, B_ϕ are the covariant components of the magnetic field, and ι is the rotational transform. We restrict ourselves to a simple model of the equilibrium, which,

however, is sufficient for studying Alfvén eigenmodes in the optimized stellarators of the Wendelstein type. Namely, we take $B_\theta = 0$ because B_θ is essentially the toroidal plasma current. In addition, we neglect the effect of the plasma pressure on the equilibrium by taking $B_\psi = 0$ and $B_\phi = \text{const}$ and neglecting ϵ_0. Then we can write the following relationships:

$$B^2 J = \text{const}, \quad b^\phi = b^\theta \iota^{-1} = \frac{h}{R_0}, \quad \nabla_\parallel = \frac{h}{R_0}\hat{L}, \quad \hat{L} = \iota\frac{\partial}{\partial\theta} + \frac{\partial}{\partial\phi}, \tag{18}$$

where $h = 1+\epsilon_m \cos N\phi+\epsilon_h \cos(N\phi-\theta)+\epsilon_t \cos\theta$, J is the Jacobian ($J^{-1} = \nabla\psi\cdot\nabla\theta\times\nabla\phi$), R_0 is the large radius of the torus defined by $B_\phi = \bar{B}R_0$.

Using Eq. (18) and approximating the magnetic field line curvature as $\vec{\mathcal{K}} = B^{-1}\nabla_\perp B$, we obtain the eigenmode equation as follows (below tilde over perturbed quantities is omitted):

$$\hat{L}\frac{\partial}{\partial x^j}\left(\nabla_\perp \hat{L}\Phi\right)^j + \omega^2 R_0^2 \frac{\partial}{\partial x^j}\frac{(\nabla_\perp\Phi)^j}{\bar{v}_A^2 h^4} = 0, \tag{19}$$

where $x^j = \psi, \theta, \phi$; the subscripts and superscripts j label the co- and contravariant vector components, $\bar{v}_A = \bar{B}/(4\pi\rho)$ (note that here and below we imply summation over repeating indices). Equation (19) can be presented in another form by expanding the perturbation $\tilde{\Phi}$ in a Fourier series,

$$\Phi = \sum_{m,n} \Phi_{mn}(\psi)\exp(im\theta - in\phi - i\omega t), \tag{20}$$

where m and n are the poloidal and toroidal mode numbers, respectively. Then, using the fact that

$$(\nabla_\perp\Phi)^i = \sum_{m,n}\left(g^{ij}\frac{\partial}{\partial x^j} - b^i i k_\parallel h\right)\Phi_{m,n}\exp(im\theta - in\phi - i\omega t), \tag{21}$$

where $k_\parallel = (m\iota - n)/R_0$ is the longitudinal wavenumber, and substituting Eq. (21) to Eq. (19), we get:

$$\sum_{m,n}\left[\hat{L}\frac{\partial}{\partial x^i}\left(g^{i\psi}k_\parallel{}' + k_\parallel g^{ij}\frac{\partial}{\partial x^j} - ihk_\parallel{}^2 b^i\right)\right.$$
$$\left. -\omega^2 R_0 \frac{\partial}{\partial x^i}\frac{1}{\bar{v}_A^2 h^4}\left(ig^{ij}\frac{\partial}{\partial x^i} + hb^i k_\parallel\right)\right]\Phi_{m,n}\exp(im\theta - in\phi - i\omega t) = 0. \tag{22}$$

Equations (19), (22) describe all shear Alfvén modes, but they neglect the influence of the sound spectrum, which may be of importance in the low frequency range. These equations are three-dimensional. In particular, in Eq. (22) the dependence on θ and ϕ arises not only because of Fourier harmonics of B but also from the metric tensor coefficients. However, for the most part, the $\mathcal{O}(\epsilon)$ terms weakly affect the Alfvén waves, where ϵ denotes both normalized Fourier harmonics in Eq. (15) and the corresponding terms in the metric tensor component $g^{\psi\psi}$, see Sec. III. The exception are those terms in the eigenmode equation which involve $\partial^2\Phi/\partial\psi^2$ because the coefficient of the second derivative of Φ, as will be seen later, vanishes when $\omega = k_\parallel v_A(\psi)$ and $\epsilon = 0$. Assuming ϵ to be small, we reduce Eq. (22) to a set of weakly coupled one-dimensional equations. With this purpose we use the expressions for the metric tensor components derived in Appendix A, Eqs. (A39)–(A44). The estimates of the magnitudes of the components given by Eqs. (A51) and (A52) show that the terms including $g^{\psi\phi}$, $g^{\theta\phi}$, and $g^{\phi\phi}$ in Eq. (22) are R_0^2/r^2 (r is the radial flux coordinate defined by the equation $\psi = \bar{B}r^2/2$) times less than those including $g^{\psi\psi}$, $g^{\psi\theta}$, and $g^{\theta\theta}$. In our analysis, we neglect these terms and retain $\mathcal{O}(\epsilon)$ contributions only in the $g^{\psi\psi}$ component, which enters the terms involving the second-order radial derivative of the wave function. Then, using Eqs. (A39)–(A44), we write:

$$g^{\psi\psi} = 2\psi\delta_0\bar{B}h_g, \quad g^{\theta\theta} = \delta_0\bar{B}/(2\psi) \quad g^{\psi\theta} \approx g^{\psi\phi} \approx g^{\theta\phi} \approx g^{\phi\phi} \approx 0,$$
$$h_g = 1 + \sum_{\mu\nu} \epsilon_g^{(\mu\nu)} \cos(\mu\theta - \nu N\phi), \tag{23}$$

$$B = \bar{B}h, \quad h = 1 + \sum_{\mu,\nu} \epsilon_B^{(\mu\nu)} \cos(\mu\theta - \nu N\phi), \tag{24}$$

where

$$\epsilon_B^{(01)} = \epsilon_m, \quad \epsilon_B^{(11)} = \epsilon_h, \quad \epsilon_B^{(10)} = \epsilon_t, \tag{25}$$

μ and ν are integers, $\delta_0 = \delta_0(\kappa)$, κ is the elongation of the plasma cross section, the dependence of δ on κ and $\epsilon_g^{(\mu\nu)}$ will be specified later (in Sec. III). Due to these relations, Eq. (22) can be presented as follows (δ_0 is assumed to be constant):

$$\sum_{m,n}\sum_{\mu,\nu}\left\{\frac{1}{r}\frac{\partial}{\partial r}r\left[\left(k_\parallel^2-\frac{\omega^2}{\bar{v}_A^2}\right)\left(1+\epsilon_g^{(\mu\nu)}\cos(\mu\theta-\nu N\phi)\right)\right.\right.$$
$$\left.+4\epsilon_B^{(\mu\nu)}\frac{\omega^2}{\bar{v}_A^2}\cos\left(\mu\theta-\nu N\phi\right)-i\epsilon_g^{(\mu\nu)}\frac{k_\parallel}{R_0}(\nu N-\mu\iota)\sin\left(\mu\theta-\nu N\phi\right)\right]\frac{\partial}{\partial r}$$
$$\left.+\left[\left(k_\parallel^2-\frac{\omega^2}{\bar{v}_A^2}\right)\left(\frac{k_\parallel^2}{\delta_0}-\frac{m^2}{r^2}\right)+\frac{k_\parallel}{r}(rk_\parallel')'\right]\right\}\Phi_{m,n}\exp(im\theta-in\phi-i\omega t)=0, \tag{26}$$

where primes denote radial derivatives, d/dr. We neglect the terms including the radial derivative of $k_\parallel$ since, as one can show, they are smaller by a factor of r^2/R_0^2 than the term $k_\parallel^2 m^2/r^2$ if the radial variation of the rotational transform is weak, $\iota(r)=\iota_0+\iota_2(r/R_0)^2$, which was assumed during the derivation of the metric tensor in Appendix A. Then, proceeding to a new wave function, $E=\Phi/r$, we transform Eq. (26) into the following equation:

$$\sum_{m,n}\sum_{\mu,\nu}\left\{\frac{\partial}{\partial r}r^3\left[\left(\frac{\omega^2}{\bar{v}_A^2}-k_\parallel^2\right)\left(1+\epsilon_g^{(\mu\nu)}\cos\left(\mu\theta-\nu N\phi\right)\right)\right.\right.$$
$$\left.-4\epsilon_B^{(\mu\nu)}\frac{\omega^2}{\bar{v}_A^2}\cos\left(\mu\theta-\nu N\phi\right)+i\epsilon_g^{(\mu\nu)}\frac{k_\parallel}{R_0}(\nu N-\mu\iota)\sin\left(\mu\theta-\nu N\phi\right)\right]\frac{\partial}{\partial r}$$
$$\left.+\left[r\left(\frac{\omega^2}{\bar{v}_A^2}-k_\parallel^2\right)\left(1-m^2\right)+r^2\left(\frac{\omega^2}{\bar{v}_A^2}\right)'\right]\right\}E_{m,n}\exp(im\theta-in\phi-i\omega t)=0. \tag{27}$$

Equation (27) yields the infinite set of second-order one-dimensional differential equations for the wave amplitudes $E_{m,n}$:

$$\sum_{\mu,\nu}\left\{\frac{\partial}{\partial r}r^3\left(\frac{\omega^2}{\bar{v}_A^2}-k_{m,n}^2\right)\frac{\partial E_{m,n}}{\partial r}+Q_{m,n}E_{m,n}\right.$$
$$+\frac{\partial}{\partial r}r^3\left[\frac{\omega^2}{\bar{v}_A^2}\left(\frac{\epsilon_g^{(\mu\nu)}}{2}-2\epsilon_B^{(\mu\nu)}\right)-k_{m,n}k_{m+\mu,n+\nu N}\frac{\epsilon_g^{(\mu\nu)}}{2}\right]\frac{\partial E_{m+\mu,n+\nu N}}{\partial r}$$
$$\left.+\frac{\partial}{\partial r}r^3\left[\frac{\omega^2}{\bar{v}_A^2}\left(\frac{\epsilon_g^{(\mu\nu)}}{2}-2\epsilon_B^{(\mu\nu)}\right)-k_{m,n}k_{m-\mu,n-\nu N}\frac{\epsilon_g^{(\mu\nu)}}{2}\right]\frac{\partial E_{m-\mu,n-\nu N}}{\partial r}\right\}=0, \tag{28}$$

where $k_{m,n}\equiv k_\parallel(m,n)$,

$$Q_{m,n}=r\left(\frac{\omega^2}{\bar{v}_A^2}-k_{m,n}^2\right)(1-m^2)+r^2\left(\frac{\omega^2}{\bar{v}_A^2}\right)'. \tag{29}$$

The coupling due to helicity, toroidicity, etc. may involve sets of modes with different mode numbers, in which case the sets are independent, i.e., one can consider independently pairs of equations coupled because of the mirror modulation of the magnetic field, the helicity, etc. However, this procedure is valid only when ϵ_α is sufficiently small. Otherwise, a more complicated analysis is required to study AEs.

III. KINDS OF ALFVÉN EIGENMODES IN HELIAS CONFIGURATIONS. CHARACTERISTIC FREQUENCIES.

One can expect that the presence of several Fourier harmonics in the magnetic field strength of the Helias configurations and the strong non-circularity of the plasma cross-section, which varies along the large azimuth of the torus, will result in several gaps in the Alfvén continuum, where discrete modes can reside.

In this section we clarify what types of gaps and AEs are possible in a Helias. To do it, we assume that the Fourier harmonics of the magnetic field strength and $\epsilon_g^{(\mu\nu)}$ are so small that various kinds of AEs can be considered independently. In this case, the gaps in the Alfvén continuum arise in the vicinity of the local Alfvén wave frequencies, $\omega(r) = |k_\parallel| v_A$, at which the frequencies of two modes with different mode numbers would coincide [$\omega_{m,n}(r_*) = \omega_{m+\mu,n+\nu N}(r_*)$, where r_* is determined by the latter equation] if $\epsilon^{(\mu\nu)}$, i.e, the factor providing the coupling, were absent. In the presence of the coupling factor, the branches $\omega_{m,n}(r)$ and $\omega_{m+\mu,n+\nu N}(r)$ unite above and below $\omega(r_*)$ in the vicinity of r_*, producing a gap with the width of the order of $\epsilon^{(\mu\nu)}$. These frequencies and the characteristic magnitudes of the rotational transform ι_* associated with the Fourier harmonics in Eq. (15) are as follows (we consider $\omega > 0$):

$$\omega_{m,n}^{m+1,n} = \frac{\iota_* v_{A*}}{2R_0}, \quad \iota_* = \frac{n}{m+1/2} \quad \text{for TAE}, \tag{30}$$

$$\omega_{m,n}^{m+1,n+N} = \frac{N v_{A*}}{2R_0}\left(1 - \frac{\iota_*}{N}\right), \quad \iota_* = \frac{n+N/2}{m+1/2} \quad \text{for HAE}_{11}, \tag{31}$$

$$\omega_{m,n}^{m,n+N} = \frac{N v_{A*}}{2R_0}, \quad \iota_* = \frac{n+N/2}{m} \quad \text{for MAE}, \tag{32}$$

where the subscripts and superscripts at ω shows the mode numbers of the coupled modes, $v_{A*} = v_A(r_*)$. The first of these equations determines the characteristic frequency of the well-known toroidicity-induced Alfvén eigenmodes (TAE). The second one determines the frequency of the helicity-induced Alfvén eigenmodes arising due to the presence of $\epsilon_B^{(11)} \equiv \epsilon_h$. We refer to this mode as HAE_{11}, where the first and second subscripts show

the magnitude of μ and ν, respectively. At last, Eq. (32) is relevant to mirror-induced Alfvén eigenmodes (MAE) associated with the presence of ϵ_m.

In order to find other kinds of AEs, we analyze the effects of the rotation and varying elongation of the plasma cross section on the mode coupling. With this purpose, we have to consider the metric tensor component $g^{\psi\psi}$, which is contained in the coefficient at $\partial^2\Phi/\partial\psi^2$. Using Eqs. (A39), (A45), we write:

$$g^{\psi\psi} = 2B_0(\phi)\{\delta(\phi) + \lambda(\phi)\cos[2\theta - 2\theta_0(\phi)]\}\psi, \tag{33}$$

where $B_0(\phi) = \bar{B}[1 + \epsilon_m \cos(N\phi)]$ is the magnetic field at the magnetic axis,

$$\delta(\phi) = \frac{\kappa(\phi) + \kappa(\phi)^{-1}}{2}, \quad \lambda(\phi) = -\frac{\kappa(\phi) - \kappa(\phi)^{-1}}{2}. \tag{34}$$

We assume that the plasma cross section rotates along ϕ in such a way that it turns by π in the poloidal direction for a field period ($\Delta\phi = 2\pi/N$), which is the case in W7-X [33] and in a Helias reactor [25]. Then we can take $\theta_0(\phi) = N\phi/2$. In addition, we allow for the fact that the elongation varies with ϕ, being maximum at the toroidal angles where the magnetic field strength is maximum. Then we can write

$$\delta(\phi) = \delta_0 + \delta_1 \cos N\phi, \quad \lambda(\phi) = \lambda_0 + \lambda_1 \cos N\phi, \tag{35}$$

where

$$\delta_0 = \frac{1}{2}(\delta_{max} + \delta_{min}), \quad \delta_1 = \frac{1}{2}(\delta_{max} - \delta_{min}), \tag{36}$$

$$\lambda_0 = -\frac{1}{2}(|\lambda|_{max} + |\lambda|_{min}), \quad \lambda_1 = -\frac{1}{2}(|\lambda|_{max} - |\lambda|_{min}), \tag{37}$$

the subscripts "max" and "min" refer to the maximum and minimum magnitudes of the elongation, respectively. Using Eqs. (33)–(37), we obtain:

$$\begin{aligned} g^{\psi\psi} = 2\psi\bar{B}\delta_0 \Big[1 &+ \epsilon_g^{(01)}\cos(N\phi) + \epsilon_g^{(21)}\cos(2\theta - N\phi) \\ &+ \epsilon_g^{(22)}\cos(2\theta - 2N\phi) + \epsilon_g^{(20)}\cos(2\theta)\Big], \end{aligned} \tag{38}$$

where $\epsilon_g^{(01)} = \epsilon_m + \delta_1/\delta_2 > 0$ is the factor producing the mirror mode coupling, $\epsilon_g^{(21)} = \lambda_0/\delta_0 < 0$ and $\epsilon_g^{(22)} = \lambda_1/(2\delta_0) < 0$ are the factors producing the helical coupling, $\epsilon_g =$

$\lambda_1/(2\delta_0) < 0$ produces the ellipticity-induced gap. In particular, taking $\kappa_{min} = 1.5$, $\kappa_{max} = 3.6$, $\epsilon_m = 0.1$, we obtain: $\delta_{min} = 1.08$, $\delta_{max} = 1.94$; $|\lambda|_{min} = 0.42$, $|\lambda|_{max} = 1.66$; $\delta_0 = 1.51$, $\delta_1 = 0.43$; $\lambda_0 = -1.04$, $\lambda_1 = -0.62$. This yields $\epsilon_g^{(01)} = 0.38$, $\epsilon_g^{(21)} = -0.68$, $\epsilon_g^{(22)} = \epsilon_g^{(20)} = -0.2$.

Comparing the amplitudes of various harmonics in Eq. (38) with the amplitudes in the Fourier spectrum of B_0 (the dominant harmonic in the plasma core is $\epsilon_m \sim 0.1$ [25,33]), we conclude that the rotation of the plasma cross section and the variation of the elongation with ϕ are expected to produce stronger mode coupling than the harmonics of the magnetic field B_0. Especially strong coupling is associated with the rotation of the cross section, which is responsible for the harmonic with $\epsilon_g^{(21)}$ coupling the modes with m, n and $m+2, n+N$ mode numbers. We will refer to the modes that can arise within the gap associated with $\epsilon_g^{(21)}$ as HAE_{21}. The variation of the magnitude of the elongation contributes to the MAE gap and, in addition, produces the HAE_{22} gap (associated with coupling of the modes m, n and $m+2$, $n+2N$) and the ellipticity-induced gap (with EAE modes) known from tokamak research. Note that the nature of the coupling parameters leading to EAEs in tokamaks and Helias systems is different: the $\mu = 2$, $\nu = 0$ coupling results from the cross-section elongation in tokamaks and from the joint action of rotation and toroidal variation of the elongation in Helias systems.

The consideration above enables us to add the following characteristic frequencies and rotational transforms associated with various terms in Eq. (38):

$$\omega_{m,n}^{m+2,n+N} = \frac{N v_{A*}}{2R_0}\left(1 - \frac{2\iota_*}{N}\right), \quad \iota_* = \frac{n + N/2}{m+1} \quad \text{for } \mathrm{HAE}_{21}, \tag{39}$$

$$\omega_{m,n}^{m+2,n+2N} = \frac{N v_{A*}}{R_0}\left(1 - \frac{\iota_*}{N}\right), \quad \iota_* = \frac{n+N}{m+1}, \quad \text{for } \mathrm{HAE}_{22}, \tag{40}$$

$$\omega_{m,n}^{m+2,n} = \frac{\iota_* v_{A*}}{R_0}, \quad \iota_* = \frac{n}{m+1} \quad \text{for EAE}. \tag{41}$$

In general, when the modes m, n and $m+\mu$, $n+\nu N$ are coupled,

$$\omega_{m,n}^{m+\mu,n+\nu N} = (N\nu - \mu\iota_*)\frac{v_{A*}}{2R_0}, \quad \iota_* = \frac{2n + \nu N}{2m + \mu}. \tag{42}$$

Equation (42) can be useful because, in reality, the family of gaps and corresponding characteristic frequencies of AEs in the Helias configurations are richer than those given by Eqs. (30)–(32), (39)–(41) for two reasons. First, Eq. (15) does not take into account all Fourier harmonics, and $g^{\psi\psi}$ given by Eq. (38) does not include all possible terms (e.g., terms associated with the triangularity of the plasma cross section). Second, secondary and higher-order gaps may be essential when $\epsilon^{(\mu\nu)}$ is not too small. We mean the following. When $|k_{m,n}(r_*)| = |k_{m+\mu,n+\nu N}(r_*)|$, the modes with m, n and $m+\mu$, $n+\nu N$ can be coupled, and the gap would arise even in the case of $\epsilon^{(\mu\nu)} = 0$ provided that both these modes were coupled with one or more other modes through some other coupling parameters; for instance, these would be the case if $\epsilon^{(\mu/2,\nu/2)}$ did not vanish, providing the coupling through the $m + \mu/2$, $N + \nu N/2$ mode. The higher-order gaps have the width of the order of ϵ^σ with $\sigma > 1$ (for the secondary gaps, $\sigma = 2$, which will be shown in Sec. V). In particular, as $\epsilon_g^{(21)}$ is relatively large, one may expect that HAE_{42} gap will be rather large; its width can be estimated as the square of the HAE_{21} width. The higher-order gaps can have the hybrid nature. For instance, the modes with m, n and m, $n + 2\nu$ can be coupled due to the presence of the helicity ($\epsilon^{(22)}$) and ellipticity ($\epsilon^{(20)}$); furthermore, in this case the modes can be coupled through the mirror parameter, ϵ_m. In order to refer to hybrid modes we will use the notation "$\mathrm{AE}_{\mu\nu}$", where the subscripts indicate that the gap is associated with the intersection of the m, n and $m + \mu$, $n + \nu N$ branches of the cylindrical continuum. Note that the MAE gap ($\mu = 0$, $\nu = 1$) arises not only from the direct interaction of the m, n and m, $n + N$ modes through the coupling parameter ϵ_m but also from the interaction via the $m+2$, $n+2N$ modes due to the presence of the $\epsilon^{(21)}$, $\epsilon^{(22)}$ terms $[(m, n) \to (m + 2, n + 2N) \to (m, n + N)]$, which yields a correction to the width of the order of $\epsilon^{(21)}\epsilon^{(22)}$. Moreover, one can see that a joint action of the helicity and ellipticity also contributes to MAE gap $[(m, n) \to (m, n+N) \to (m-2, n) \to (m, n)]$, giving a correction of the order of $\epsilon^{(20)}\epsilon^{(21)}$. These corrections are essential because $\epsilon^{(21)}$ is rather large. Nevertheless, we will refer to the (0,1) gap and the corresponding eigenmodes as "MAE" because it is ϵ_m that is responsible for the direct mode interaction.

The family of characteristic frequencies determined by Eqs. (32)–(30) and Eqs. (39)–

(41) is presented in Fig. 1. We observe that the frequencies corresponding to different kinds of AEs are well separated in a Helias reactor with $\iota \sim 1$. But this fact is not sufficient to understand whether the different kinds of AEs are really independent on each other because the gaps corresponding to them may be large.

The weak magnetic shear of Helias configurations essentially restricts the wave numbers of the coupled modes. To find them, we use ι_* given by Eqs. (30)–(32), (39)–(41) and the rotation transform $\iota(\psi)$ relevant to a Helias reactor (see Fig. 2) [25,37]. The results are presented in Fig. 3. It follows from Fig. 3 that when the wave numbers are small, typically only one pair of modes is coupled in Alfvén eigenmodes of a certain kind; when the wave numbers are sufficiently large, few modes with successive numbers can be coupled at different radii.

IV. GAPS IN ALFVÉN CONTINUUM IN THE APPROXIMATION OF WEAKLY COUPLED MODES.

Let us assume that the continuum gaps are narrow so that the AEs residing in different gaps can be treated independently, in which case Eq. (28) is reduced to a pair of equations describing two coupled harmonics in a gap. Later, after obtaining the equations, we will see whether this assumption is justified.

Assuming that two modes with the wavenumbers m, n and $m+\mu$, $n+\nu N$ are coupled, we obtain from Eq. (28):

$$\frac{\partial}{\partial r} r^3 \left(\frac{\omega^2}{\bar{v}_A^2} - k_{m,n}^2 \right) \frac{\partial E_{m,n}}{\partial r} + Q_{m,n} E_{m,n}$$
$$+ \frac{\partial}{\partial r} r^3 \left[\frac{\omega^2}{\bar{v}_A^2} \left(\frac{\epsilon_g^{(\mu\nu)}}{2} - 2\epsilon_B^{(\mu\nu)} \right) - k_{m,n} k_{m+\mu,n+\nu N} \frac{\epsilon_g^{(\mu\nu)}}{2} \right] \frac{\partial E_{m+\mu,n+\nu N}}{\partial r} = 0, \tag{43}$$

$$\frac{\partial}{\partial r} r^3 \left(\frac{\omega^2}{\bar{v}_A^2} - k_{m+\mu,n+\nu N}^2 \right) \frac{\partial E_{m+\mu,n+\nu N}}{\partial r} + Q_{m+\mu,n+\nu N} E_{m+\mu,n+\nu N}$$
$$+ \frac{\partial}{\partial r} r^3 \left[\frac{\omega^2}{\bar{v}_A^2} \left(\frac{\epsilon_g^{(\mu\nu)}}{2} - 2\epsilon_B^{(\mu\nu)} \right) - k_{m,n} k_{m+\mu,n+\nu N} \frac{\epsilon_g^{(\mu\nu)}}{2} \right] \frac{\partial E_{m,n}}{\partial r} = 0. \tag{44}$$

If ϵ_B and ϵ_g vanished, the modes $E_{m,n}$ and $E_{m+\mu,n+\nu N}$ would be decoupled. Then Eqs. (43), (44) would have singularities at $\omega_1 = |k_{m,n}| \bar{v}_A$ and $\omega_2 = |k_{m+\mu,n+\nu N}| \bar{v}_A$, respec-

tively. These two equations determine two cylindrical Alfvén wave continua. In fact, the presence of the terms with ϵ_B, ϵ_g breaks the cylindrical continua in the point where the cylindrical branches intersect and creates two new continua. The Helias continua in the approximation of the small gap width are determined by the equation $D = 0$, where D is the determinant of the coefficients of the second order derivative terms in Eqs. (43), (44). Using the equation $D = 0$, we find that the relative half-width of the frequency gap at r_*, where the cylindrical continua intersect, is

$$G \equiv \frac{\Delta\omega}{\omega(r_*)} = \left| \epsilon_B^{(\mu\nu)} - \frac{\epsilon_g^{(\mu\nu)}}{2} \right|, \tag{45}$$

where $\Delta\omega$ is the absolute half-width of a gap. Using this equation and the numerical estimates of ϵ given in Sec. III we find that $G = 0.34$ for HAE_{21}, $G = 0.1$ for HAE_{22} and EAE, and $G = 0.09$ for MAE. The width of the TAE and HAE_{11} gaps cannot be determined here because the corresponding contributions to the metric tensor is not calculated in this work. Note that the contributions of the mirror harmonics of the magnetic field strength and the metric tensor are of different signs; therefore, their joint action reduces the gap.

Now we can clarify whether our assumption that the gaps are narrow is justified. With this purpose we compare the half-width of the HAE_{21} gap, which is the largest, and the distance between $\omega_{m,n}^{m+2,n+N}$ and its neighbors, in particular, $\omega_{m,n}^{m+1,n+N}$ (HAE_{11}) and $\omega_{m,n}^{m,n+N}$ (MAE). Taking into account that they weakly change in a Helias reactor and neglecting the effect of the plasma inhomogeneity, we obtain:

$$\frac{G^{HAE_{21}}\omega^{m+2,n+N}}{\omega_{m,n}^{m+1,n+N} - \omega_{m,n}^{m+2,n+N}} \approx 2\frac{G^{HAE_{21}}\omega^{m+2,n+N}}{\omega_{m,n}^{m,n+N} - \omega_{m,n}^{m+2,n+N}} \approx \left(\frac{N}{2\iota_*} - 1\right)\left|\epsilon_g^{(21)}\right|. \tag{46}$$

For $N = 5$, $|\epsilon_g^{(21)}| = 0.68$, we find that the first ratio exceeds unity for $\iota < 1$. Furthermore, the second ratio also exceeds unity unless $\iota < 0.6$. On the other hand, the distance between the HAE_{21} and its low frequency neighbors, EAE and TAE gaps, is rather large for $\iota \ll 1$, and, therefore, HAE_{21} and EAE weakly affect each other in this case.

We can conclude that the assumption made above that various kinds of AEs can be treated independently, in general, is not justified for the Helias configurations. Moreover,

a question arises whether any continuum survives when frequency gaps determined by Eqs. (43), (44) for various μ, ν overlap.

To understand what happens with continuum gaps in this situation, at first, let us see how the HAE_{21} gap will change under the influence of neighboring harmonics. With this purpose we consider the interaction of the following harmonics:

$$m-2, n-N \Longleftrightarrow m, n \Longleftrightarrow m+2, n+N \Longleftrightarrow m+4, n+2N. \tag{47}$$

In this case the equation $D=0$ is

$$\begin{vmatrix} \Omega^2_{m-2,n-N} & \mathcal{H}^{m,n}_{m-2,n-N} & 0 & 0 \\ \mathcal{H}^{m,n}_{m-2,n-N} & \Omega^2_{m,n} & \mathcal{H}^{m+2,n+N}_{m,n} & 0 \\ 0 & \mathcal{H}^{m+2,n+N}_{m,n} & \Omega^2_{m+2,n+N} & \mathcal{H}^{m+4,n+2N}_{m+2,n+N} \\ 0 & 0 & \mathcal{H}^{m+4,n+2N}_{m+2,n+N} & \Omega^2_{m+4,n+2N} \end{vmatrix} = 0, \tag{48}$$

where

$$\Omega^2_{m,n} \equiv \omega^2 - k^2_{m,n}\bar{v}^2_A, \quad \mathcal{H}^{m+p,n+q}_{m,n} \equiv (\omega^2 - k_{m,n}k_{m+p,n+q}\bar{v}^2_A)\frac{\epsilon^{(21)}_g}{2}. \tag{49}$$

We study the effect of the $m-2, n-N$ and $m+4, n+2N$ harmonics on the gap at r_* in the vicinity of $\omega^{m+2,n+N}_{m,n}$ perturbatively by seeking for a solution of Eq. (48) in the form:

$$\omega = \omega_0 + \delta\omega, \tag{50}$$

where ω_0 is the solution in the absence of the $m+4, n+2N$ and $m-2, n-N$ harmonics, $\delta\omega$ is the correction associated with their presence. Correspondingly, we write Eq. (48) as:

$$\Lambda(\omega) = \lambda(\omega) \tag{51}$$

where $\Lambda = \Omega^2_{m,n}\Omega^2_{m+2,n+N} - (\mathcal{H}^{m+2,n+N}_{m,n})^2$, λ is the correction. The solution of Eq. (51) is

$$\delta\omega = \frac{\lambda(\omega_0)}{\partial\Lambda/\partial\omega|_{\omega_0}} \tag{52}$$

with ω_0 determined by the equation $\Lambda(\omega_0) = 0$. Noting that $\omega_{m-2,n-N} = \omega_{m+4,n+2N}$, we find:

$$\omega_0 = k_{*h}\bar{v}_A\left(\frac{2\pm\epsilon_g^{(21)}}{2\mp\epsilon_g^{(21)}}\right)^{1/2}, \quad \delta\omega = -k_{*h}\bar{v}_A\frac{\left(\epsilon_g^{(21)}\right)^2}{16} + \mathcal{O}(\epsilon^3), \tag{53}$$

where $k_{*h} = (N/2 - \iota_*)/R_0$, the subscript "$h$" meaning "helical". It follows from Eq. (53) that the multiple mode interaction displaces the HAE_{21} gap down, but this displacement is rather small.

Now we proceed to the study of the interaction between the gaps. We consider the influence of HAE_{21} gap on the MAE gap arising from the intersection of the cylindrical continua of modes with m, n and $m, n + N$. The presence of the term with $\epsilon_g^{(21)}$ in Eq. (28) affects the MAE gap, first of all, through the interaction with the $m \pm 2, n \pm N$ and $m \pm 2, n + N \pm N$ modes. The roles of these modes are different. The most important are the $m + 2, n + N$ and $m - 2, n$ modes because their frequencies are closer to the MAE gap (this follows from the fact that $k_{m,n} = -k_{m,n+N} = N/(2R_0)$, $k_{m-2,n} = -k_{m+2,n+N} = (N/2 - 2\iota)/R_0$, $k_{m-2,n-N} = -k_{m+2,n+2N} = (1.5N - 2\iota)/R_0$ for $r = r_*$). Therefore, restricting ourselves to the analysis of the four-wave interaction, we consider the following modes:

$$m + 2, n + N \Longleftrightarrow m, n \Longleftrightarrow m, n + N \Longleftrightarrow m - 2, n. \tag{54}$$

Then the equation $D = 0$ yields:

$$\begin{vmatrix} \Omega^2_{m+2,n+N} & \mathcal{H}^{m+2,n+N}_{m,n} & 0 & 0 \\ \mathcal{H}^{m+2,n+N}_{m,n} & \Omega^2_{m,n} & \mathcal{M} & 0 \\ 0 & \mathcal{M} & \Omega^2_{m,n+N} & \mathcal{H}^{m,n+N}_{m-2,n} \\ 0 & 0 & \mathcal{H}^{m,n+N}_{m-2,n} & \Omega^2_{m-2,n} \end{vmatrix} = 0, \tag{55}$$

where

$$\mathcal{M} = \omega^2\left(\frac{\epsilon_g^{(01)}}{2} - 2\epsilon_m\right) - \frac{\epsilon_g^{(01)}}{2}k_{m,n}k_{m,n+N}\bar{v}_A^2. \tag{56}$$

Equation (55) can be presented in the form of Eq. (51) with λ describing the influence of the $m - 2, n$ and $m + 2, n + N$ modes on the MAE gap. Then, neglecting the terms of the order of $(\epsilon_g^{(21)})^4$, we have for $r = r_*$:

$$\Lambda(\omega) = \Omega_{m,n}^4 - \mathcal{M}^2, \quad \lambda(\omega) = 2\mathcal{H}^2 \frac{\Omega_{m,n}^2}{\Omega_{m-2,n}^2} \tag{57}$$

where $\mathcal{H} \equiv \mathcal{H}_{m-2,n}^{m,n} = \mathcal{H}_{m,n}^{m+2,n+N}$. A solution can be found according to Eqs. (50), (52). We obtain:

$$\omega_0 = k_{*m}\bar{v}_A \left(\frac{1 \pm \epsilon_g^{(01)}/2}{1 \mp \epsilon_g^{(01)}/2 \pm 2\epsilon_m} \right)^{1/2}, \quad \delta\omega = k_{*m}\bar{v}_A \frac{\left(\epsilon_g^{(21)}\right)^2}{8} \frac{k_{*m} + k_1}{k_{*m} - k_1} + \mathcal{O}(\epsilon^3), \tag{58}$$

where $k_{*m} = N/(2R_0)$, the subscript "m" meaning "mirror"; $k_1 = (N/2 - 2\iota_*)/R_0$, ι_* is given by Eq. (32). We conclude that the MAE gap is displaced up by the HAE_{21} coupling. Taking $N = 5$, $\epsilon_g^{(21)} = 0.68$, $\iota_* = 0.9$, we obtain $\delta\omega/(k_{*m}\bar{v}_A) \approx 10\%$.

Thus, the influence of higher-order interactions on the continuum gaps is clear on the qualitative level. The gaps "repel" each other, tending to prevent their overlap. To understand the structure of the continuum gaps more definitely, we need to involve numerical methods. This will be done in the next section.

V. STRUCTURE OF THE ALFVÉN CONTINUUM IN HELIAS CONFIGURATIONS

The aim of this section is to develop a method for finding the structure of the shear Alfvén continuum in a general three-dimensional toroidal magnetic configuration. We proceed from the general equation of the Alfvén oscillations, Eq. (19), which we can re-write for our purposes as follows:

$$\hat{L}\frac{\partial}{\partial x^i}\left[g_\perp^{ij}\frac{\partial}{\partial x^j}\left(\hat{L}\Phi\right)\right] + \omega^2 R_0^2 \frac{\partial}{\partial x^i}\left(\frac{g_\perp^{ij}}{\bar{v}_A^2 h^4}\frac{\partial \Phi}{\partial x^j}\right) = 0, \tag{59}$$

where $g_\perp^{ij} = g^{ij} - b^i b^j$.

An equation describing the continuous spectrum of Eq. (59) can be easily written intuitively, using the similarity with the spectra of systems of ordinary differential equations described in the previous section (more rigorous substantiation of the equation to be obtained is given in Appendix B). In the above examples of eigenvalue problems, the continuous spectrum consisted of the values of ω for which the matrix coefficient at the highest-order radial derivative is degenerate at a certain radial point, $D = 0$, which

typically results in singularity of solutions at this point. In other words, ω belongs to the continuum if it is an eigenvalue of the problem $\mathcal{G}(\psi)\Phi - \omega^2\mathcal{C}(\psi)\Phi = 0$ at certain ψ, where $\mathcal{G}(\psi) - \omega^2\mathcal{C}(\psi)$ is the matrix coefficient at the second radial derivative in the considered system of differential equations, Φ is understood as the column of the amplitudes of the considered modes. Similarly, in a general case, one can conclude that ω belongs to the continuous spectrum of Eq. (59) if there is a radial point ψ at which ω is an eigenvalue of the equation

$$\hat{L}\left(g^{\psi\psi}\hat{L}\Phi\right) + \omega^2 R_0^2 \frac{g^{\psi\psi}}{\bar{v}_A^2 h^4}\Phi = 0 \tag{60}$$

with the natural boundary condition of periodicity. The linear differential operator entering this equation is, in fact, the "operator coefficient" at the second radial derivative in Eq. (59). One can say that Eq. (60) describes the propagation of Alfvén waves at a "separate" flux surface. It includes only differentiation within the flux surface (by angular variables) with ψ considered as a parameter. Its eigenvalues are functions of ψ and produce branches of the continuum as ψ is varied.

Keeping only one oscillating harmonic in $g^{\psi\psi}$ and B and presenting Φ in Eq. (60) as a sum of two coupled harmonics, one can easily re-obtain the continuum gap width given by Eq. (45). Keeping more than two harmonics of Φ, one can arrive at Eqs. (48), (55). However, when the configuration asymmetry is strong, the continuum gaps can be found only numerically.

As an arbitrary wave harmonic (m, n) can interact only with harmonics with the mode numbers $(m + \mu, n + \nu N)$, where μ and ν are integers, we take Φ in the form

$$\Phi = \sum_{\mu,\nu=-\infty}^{\infty} \Phi_{\mu\nu} \exp[i(m+\mu)\theta - i(n+\nu N)\phi] \tag{61}$$

and expand the coefficients of Eq. (60) in Fourier series:

$$g^{\psi\psi} = g_0 \left[1 + \frac{1}{2}\sum_{\mu,\nu=-\infty}^{\infty} \epsilon_g^{(\mu\nu)} \exp(i\mu\theta - i\nu N\phi)\right], \tag{62}$$

$$g^{\psi\psi}h^{-4} = g_0 \left[1 + \frac{1}{2}\sum_{\mu,\nu=-\infty}^{\infty} \epsilon_c^{(\mu\nu)} \exp(i\mu\theta - i\nu N\phi)\right], \tag{63}$$

where $\epsilon_g^{(-\mu,-\nu)} = \epsilon_g^{(\mu\nu)*}$, $\epsilon_c^{(-\mu,-\nu)} = \epsilon_c^{(\mu\nu)*}$, and the superscript "$*$" denotes complex conjugate. Note that the complex quantity $\epsilon_g^{(\mu\nu)}$ is a generalization of the corresponding quantity introduced in Eq. (23), coinciding with it when there are only cosine harmonics in the Fourier spectrum of $g^{\psi\psi}$. Then Eq. (60) is reduced to the following eigenvalue problem:

$$\sum_{\mu,\nu=-\infty}^{\infty} \mathcal{G}_{\mu_*,\nu_*;\mu,\nu}\Phi_{\mu\nu} = \omega^2 \frac{R_0^2}{\bar{v}_A^2} \sum_{\mu,\nu=-\infty}^{\infty} \mathcal{C}_{\mu_*,\nu_*;\mu,\nu}\Phi_{\mu\nu}, \tag{64}$$

where the infinite matrices $\mathcal{G}$ and $\mathcal{C}$ are given by the equations

$$\mathcal{G}_{\mu_*,\nu_*;\mu,\nu} = \left(\delta_{\mu_*\mu}\delta_{\nu_*\nu} + \frac{1}{2}\epsilon_g^{(\mu_*-\mu,\nu_*-\nu)}\right)\tilde{k}_{\mu_*\nu_*}\tilde{k}_{\mu\nu}, \tag{65}$$

$$\mathcal{C}_{\mu_*,\nu_*;\mu,\nu} = \delta_{\mu_*\mu}\delta_{\nu_*\nu} + \frac{1}{2}\epsilon_c^{(\mu_*-\mu,\nu_*-\nu)} \tag{66}$$

and are Hermitian ($\mathcal{C}_{\mu,\nu;\mu_*,\nu_*} = \mathcal{C}^*_{\mu_*,\nu_*;\mu,\nu}$, $\mathcal{G}_{\mu,\nu;\mu_*,\nu_*} = \mathcal{G}^*_{\mu_*,\nu_*;\mu,\nu}$); $\tilde{k}_{\mu\nu} = \tilde{k} + \mu\iota - \nu N$, $\tilde{k} = m\iota - n$; δ is the Kronecker symbol. Note that the elements of $\mathcal{G}$ depend on m and n only through $\tilde{k}$, and the elements of $\mathcal{C}$ do not depend on m and n at all. Thus, if modes with different mode numbers are characterized by the same values of $\tilde{k}$ for certain ι, they produce identical patterns of branches of the continuum spectrum at that ι. One the other hand, any value of $\tilde{k}$ can be reached with arbitrary accuracy by certain m and n (unless ι is rational). Due to this, we formulate the eigenvalue problem for numerical calculations in terms of $\tilde{k}$ and do not check all the time whether any given value of $\tilde{k}$ correspond to any integer m and n. Note that non-integer m and n can be interpreted as withdrawing the periodicity condition and considering waves in an infinite periodic structure, which enhances the similarity of the considered continuum gaps with Brillouin zones for the electron waves in crystals. Some consequences of the restrictions that the periodicity condition puts on continuum branches at rational flux surfaces will be discussed later.

To solve the eigenvalue problem (64) numerically, one can choose certain finite intervals in μ and ν around $\mu = 0$ and $\nu = 0$ and calculate the eigenvalues of the resulting finite-dimensional problem. If non-diagonal elements of the matrices are smaller than the diagonal ones, one can hope that those several eigenvalues for which the corresponding

eigenvectors have leading components in the central part of the chosen intervals are calculated sufficiently exactly (which can be checked by varying the length of the intervals).

This described approach was implemented in the computer code COBRA (COntinuum BRAnches). The code uses the QZ algorithm to find all eigenvalues of the generated matrix pair. An attempt to use the QR algorithm was not successful as the algorithm (or, at least, its available implementation) often fails near the rational values of ι with small denominators, when the spectrum tends to multiple degeneration. Although only one or two eigenvalues were obtained after solving one eigenvalue problem, the much faster inverse vector iteration algorithm, which gives one eigenvalue at a time, was rejected since it is hard to predict the frequency of the harmonic of interest when the perturbation is strong. Probably, methods calculating a range of spectrum would be more efficient, but they were not used for the lack of necessity (the calculation of one point of the spectrum with the ranges $-9 \le \mu \le 8$, $-5 \le \nu \le 4$, which yielded quite sufficient accuracy $< 10^{-5}$, took less than a minute on a CELERON/400 MHz desktop computer).

The code has three modes of operation. First, one can carry out scanning in $\tilde{k}$ and ι (or ψ), calculating the frequency of the continuum branch that has the largest contribution from the $\tilde{k}$ harmonic. Such scanning fills the regions outside the continuum gaps for each ι and visualizes all existing gaps at once. Second, the program can calculate the limits of the gap produced by coupling of harmonics with an arbitrary pair of "coupling numbers" (μ, ν) at various radii. With this aim, the value of $\tilde{k}$ for which the coupling takes place (i.e., $\tilde{k}_{\mu\nu} = -\tilde{k}$) is found at each radius, which is:

$$\tilde{k}_*^{(\mu,\nu)}(\iota) = (\nu N - \iota\mu)/2. \tag{67}$$

Then the calculations are performed for $\tilde{k} = \tilde{k}_*^{(\mu,\nu)}(\iota)$, after which the eigenfrequencies corresponding to the two eigenvectors with the largest $\tilde{k}$ component show the "banks" of the gap at the given radius. Third, the code can find the frequency of the continuum branch with the dominating (m, n) harmonic as a function of ι, performing the calculations for $\tilde{k} = m\iota - n$.

The obtained structure of continuum gaps for the Helias parameters is presented in

Fig. 4, where the continuum frequency normalized by the local Alfvén velocity, $\omega R_0/\bar{v}_A$, is shown versus ι. As $\bar{v}_A$, in general, depends on the plasma radius, ω after such normalization, strictly speaking, shows the real size of the continuum gaps only for the case of the constant plasma density. However, such presentation facilitates the understanding of the structure of the continuum. As described in the previous section, it is assumed that the mode coupling is caused by the harmonics of $g^{\psi\psi}$ with the numbers $(\mu, \nu) = (0, 1)$ (linked-mirror harmonic), (2,1) (HAE_{21} harmonic), (2,2) (HAE_{22} harmonic), and (2,0) (EAE harmonic). In addition, a small $(\mu, \nu) = (1, 1)$ (HAE_{11}) harmonic ($\epsilon_c^{(11)} = 0.05$) has been involved in the magnetic field strength to understand the relative position of the expected (1,1) gap (qualitative analysis of the HAE_{11} modes will be done in the next part of this work, where the corresponding harmonic of the metric tensor will be derived).

Dots in Fig. 4 show the results of the scan in ι and $\tilde{k}$ with steps 0.005 and 0.1, respectively. One can see that ω does not depend continuously on $\tilde{k}$, leaving noticeable gaps in the spectrum. The coupling numbers responsible for each gap can be easily identified. Black solid lines in the same figure, showing the calculated "banks" of each gap, indeed separate the gaps from the filled region, which proves that the identification of the nature of all visible gaps is correct. The wide grey lines show the places where the gaps would be located if the perturbation amplitude were infinitely small, $\omega R_0/\bar{v}_A = |\tilde{k}_*^{(\mu,\nu)}|$ (for comparison).

The calculations show that the actual width of the gaps is less than that expected from Eq. (45). In addition, most gaps are shifted upward or downward from their expected position, which qualitatively agrees with results of the analysis of a four-mode system in the previous subsection. The relative magnitude of the "compression" and the shift is the strongest for the gaps located near the HAE_{21} (2,1) gap, which indicates the strong influence of the (2,1) gap on its neighbors.

Nevertheless, if the characteristics frequencies of some gaps for the infinitely small coupling parameters, i.e., $\omega_{m,n}^{m+\mu,n+\nu N}$ given by Eq. (42), do not cross, the gaps remain separated by continuum "walls" even when the coupling parameters $\epsilon_{g,c}^{(\mu\nu)}$ are enough high to result in their strong displacement. Each "wall" consists of the branches of the

continuum for which $\tilde{k}$ lies between two functions $\tilde{k}_*^{(\mu,\nu)}(\iota)$ with (μ,ν) corresponding to the two gaps that the "wall" separates.

An interesting feature of the spectrum in Fig. 4 is the presence of gaps with coupling numbers (μ,ν) which are present neither in $g^{\psi\psi}$ nor in h nor in the combination $g^{\psi\psi}h^{-4}$ as they are taken for this calculation. The most probable mechanism of their formation is the three- (or more) mode interaction involving intermediate harmonics. The creation of gaps by such interaction, the possibility of which was mentioned in Sec. III, can be explained by the following example. Let the parts of the matrices $\mathcal{C}$ and $\mathcal{G}$ describing the interaction of the modes $\tilde{k}=\tilde{k}_{00}$, $\tilde{k}=\tilde{k}_{\mu_1\nu_1}$, and $\tilde{k}=\tilde{k}_{\mu_2\nu_2}$, have the form

$$\mathcal{C}=\begin{pmatrix} 1 & \epsilon_1 & 0 \\ \epsilon_1 & 1 & \epsilon_2 \\ 0 & \epsilon_2 & 1 \end{pmatrix}, \quad \mathcal{G}=\begin{pmatrix} \tilde{k}_{00}^2 & 0 & 0 \\ 0 & \tilde{k}_{\mu_1\nu_1}^2 & 0 \\ 0 & 0 & \tilde{k}_{\mu_2\nu_2}^2 \end{pmatrix}, \tag{68}$$

where ϵ_1 and ϵ_2 are arbitrary small non-zero numbers describing the coupling (for the sake of simplicity, we assume that $\mathcal{G}$ is diagonal). If $\tilde{k}_{00}=\tilde{k}_{\mu_2\nu_2}$, one can see that the interaction of these two harmonics via the $\tilde{k}_{\mu_1\nu_1}$ harmonic splits the corresponding eigenvalues by $\sim\epsilon_1\epsilon_2$ although their direct coupling is absent. An example of such gaps is the rather wide (4,2) gap in Fig. 4, which probably results from the three-mode interaction as the combination (2,1)+(2,1). Other examples are the (4,3) gap, probably arising as the combination (2,1)+(2,2), and the (0,2) gap. The width of the latter seems too wide to be accounted for by the most obvious (0,1)+(0,1) interaction; probably, the (2,2)-(2,0) combination also contributes to this gap. The large magnitude of the (2,1) harmonic of $g^{\psi\psi}$ leads to the fact that even gaps of third order in ϵ, (6,2) and (6,3), are quite noticeable. However, one should have in mind that the real width of these gaps may differ from what is calculated here as the corresponding harmonics may appear in next-order corrections to B and $g^{\psi\psi}$.

Figure 5 shows examples of the calculated continuum branches, each dominated by the harmonic with $\tilde{k}=m\iota-n$ for a certain pair of the mode numbers (m,n). As expected, the branches have discontinuities as they cross the calculated gaps. Due to the periodicity

of the configuration, the harmonics can be divided into three families, $n = 5s$, $n = 5s \pm 1$, and $n = 5s \pm 2$ (where s is an arbitrary integer), harmonics from different families not interacting with each other. For this reason, all the selected harmonics belonged to the same family ($n = 5s \pm 1$). The main aim of the calculation presented in Fig. 5 was the following. When obtaining the gap structure presented in Fig. 4, we did not see to it that the wavenumber of the dominant harmonic $\tilde{k}$ corresponds to any integer m and n. When ι is irrational, any $\tilde{k}$ can approximated with arbitrary accuracy by $m\iota - n$ for some m and n. At a rational-ι flux surface, however, $\tilde{k}$ is always a multiple of $1/l$, where l is the least denominator of ι. As, in fact, harmonics with very large m and n are of little practical importance, one could expect that those gaps for which $\tilde{k}_*^{(\mu,\nu)}$ is not a multiple of $1/l$ are effectively wider in the vicinity of this flux surface because no branches with small m and n approach the "banks" of the gaps. The calculations were intended to check if such an effect of rational ι really takes place in the analyzed Helias configuration. The rational points with the least denominators in the ι range of interest are 1 and 5/6. Figure 5 shows that the selected branches (all with m and n not exceeding 10) closely surround each gap so that no significant widening near rational points is possible. The only exception is the MAE gap which increases by three times at $\iota = 1$. However, this widening is noticeable only at $\iota > 0.96$ if the modes with $m \leq 10$ are considered. Thus, Fig. 4 correctly represents the structure of the continuum gaps, which is important, in particular, for studies of the continuum damping of Alfvén eigenmodes.

Finally, it is worth discussing why the gaps observed here are not clearly seen in recent calculations with the CAS3D3 code [28,29]. The difference in employed equilibria (we used a simple analytical approximation of the metric tensor, whereas numerical simulations of Refs. [28,29] used much more exact numerically calculated Helias equilibria) can hardly account for this (the physical mechanism producing the gaps is so transparent that there is almost no doubt that qualitatively the same picture would be observed in our calculations if we took the exact metrics). A possible explanation is the following. As mentioned above, the subroutine used to solve the eigenvalue problem in COBRA calculates all eigenvalues for a given matrix pair. As long as we plotted all the calculated eigenvalues, we obtained

false continuum branches crossing the gaps so that narrow gaps could not be visible at all. Analysis showed that the false branches were dominated by harmonics whose "partner" for the coupling responsible for the gap is absent in the mode set used by the code. Adding new harmonics to the mode set prevents these branches from crossing the gap but does not help in general since even more new branches crossing the gap appear. It seems that such false continuum branches can be found in spectra presented in Refs. [28,29]. The only solution to this problem we have found is to select the eigenvalues dominated by central harmonics of the matrix, which, of course, increases the time required for the calculations. In other words, the mode set used by the code must depend on the dominant harmonic of the branch under consideration to represent the structure of the continuum correctly. This should be taken into account when studying the continuum damping.

VI. DISCRETE EIGENMODES: HAE_{21} AND MAE MODES

In this section we will clarify whether and when discrete modes can exist in HAE_{21} and MAE gaps. Note that till now the MAE modes and even the MAE gap have not been known. The HAE_{21} modes were observed numerically in W7-X in assumption that plasma is homogeneous [28]. Here we consider both homogeneous and realistically inhomogeneous plasmas.

To solve the eigenvalue problem, we have developed the BOA (Branches Of Alfvén modes) code. The code is intended for solving the eigenvalue problem obtained by restricting Eq. (28) to a certain finite mode set. The problem is reduced to a generalized eigenvalue problem for symmetric matrices by replacing the radial derivatives with finite differences, which is solved numerically with the QZ algorithm. This code was tested on the well-known case of a TAE mode in a homogeneous plasma of a tokamak with the safety factor $q(r) = 1 + r^2/a^2$. The results are presented in Fig. 6. The shown picture coincides with that given in Ref. [38].

Let us proceed to study of the eigenmodes in a Helias reactor with the parameters given in Refs. [25,37]. In particular, we will use the ι profiles shown in Fig. 2 and the

plasma mass density profile given by

$$\rho(r) = \rho(0)\left[1 + \left(\frac{r}{ax_n}\right)^{10}\right]^{-1}, \tag{69}$$

where x_n is a parameter which will be taken either of the order unity or equal to infinity (which corresponds to homogeneous plasma), a is the plasma radius (in flux coordinates). In order to choose the wave numbers, we will employ Fig. 3. The magnitudes of the coupling parameters $\epsilon^{(\mu\nu)}$ will be taken according to Sec. III.

We begin with the HAE_{21} modes. As $\epsilon_g^{(21)}$ exceeds other coupling parameters, we neglect the effect of other kinds of AEs. In addition, we restrict ourselves to analysis of the two-wave interaction [the (m, n) and $(m+2, n+N)$ modes]. Then we can describe HAE_{21} modes by Eqs. (43), (44) with $\mu = 2$, $\nu = 1$. Results of the calculations are presented in Figs. 7–9. It follows from Fig. 7 that the gap width is rather large. The gap is open for the homogeneous plasma and the inhomogeneous plasma with $x_n = 0.9$, but it is closed for $x_n \leq 0.85$. This implies that the gap is open provided that $n(a)/n(0) \geq 1/6$. Note that the gaps for all considered x_n coincide in the region $x_n \leq 0.5$. We found that there are discrete modes inside the gap. For the case of the homogeneous plasma, two eigenmodes with the radial structure of the global character are shown in Fig. 8; their normalized eigenfrequencies ($\lambda = \omega R_0/\bar{v}_A$) are shown in Fig. 7. The eigenmode components with the higher and lower λ have the same phase and the opposite phases, respectively (in contrast to the even [39] and odd [40] core-localized TAEs). Figure 9 shows the radial structure of HAE_{21} in inhomogeneous plasma with $x_n = 0.9$. This mode has approximately the same eigenfrequency as in Fig 8, which lies just below the lower tip of the gap. The fact that the eigenfrequency intersects the continuum manifests itself only in small spikes near the plasma edge. The mode with lower λ, as in Fig. 8(b), must be strongly damped because the calculated amplitudes have large spikes in the region of continuum, see Fig. 9(b). Lowering x_n, i.e., the ratio of $n(a)/n(0)$, we found that when $x_n < 0.9$, global smooth eigenfunctions disappear.

Now we proceed to the study of the MAE modes. This requires taking into account the interaction of more than two waves because the MAE gap is essentially affected by

other gaps (see Secs. IV, V). As in Sec. IV, we consider the four-wave interaction in accordance with Eq. (54), where we add the terms describing the coupling due to $\epsilon^{(20)}$ (EAE-like coupling). Correspondingly, we use the following set of equations:

$$\begin{aligned}
&\frac{\partial}{\partial r}r^3\left(\frac{\omega^2}{\bar{v}_A^2}-k_{m,n}^2\right)\frac{\partial E_{m,n}}{\partial r}+Q_{m,n}E_{m,n}\\
&+\frac{\partial}{\partial r}r^3\left[\frac{\omega^2}{\bar{v}_A^2}\left(\frac{\epsilon_g^{(01)}}{2}-2\epsilon_m\right)-\frac{\epsilon_g^{(01)}}{2}k_{m,n}k_{m,n+N}\right]\frac{\partial E_{m,n+N}}{\partial r}\\
&+\frac{\partial}{\partial r}r^3\left(\frac{\omega^2}{\bar{v}_A^2}-k_{m,n}k_{m+2,n+N}\right)\frac{\epsilon_g^{(21)}}{2}\frac{\partial E_{m+2,n+N}}{\partial r}\\
&+\frac{\partial}{\partial r}r^3\left(\frac{\omega^2}{\bar{v}_A^2}-k_{m,n}k_{m-2,n}\right)\frac{\epsilon_g^{(20)}}{2}\frac{\partial E_{m-2,n}}{\partial r}=0
\end{aligned}\tag{70}$$

$$\begin{aligned}
&\frac{\partial}{\partial r}r^3\left(\frac{\omega^2}{\bar{v}_A^2}-k_{m,n+N}^2\right)\frac{\partial E_{m,n+N}}{\partial r}+Q_{m,n+N}E_{m,n+N}\\
&+\frac{\partial}{\partial r}r^3\left[\frac{\omega^2}{\bar{v}_A^2}\left(\frac{\epsilon_g^{(01)}}{2}-2\epsilon_m\right)-\frac{\epsilon_g^{(01)}}{2}k_{m,n}k_{m,n+N}\right]\frac{\partial E_{m,n}}{\partial r}\\
&+\frac{\partial}{\partial r}r^3\left(\frac{\omega^2}{\bar{v}_A^2}-k_{m,n+N}k_{m-2,n}\right)\frac{\epsilon_g^{(21)}}{2}\frac{\partial E_{m-2,n}}{\partial r}\\
&+\frac{\partial}{\partial r}r^3\left(\frac{\omega^2}{\bar{v}_A^2}-k_{m,n+N}k_{m+2,n+N}\right)\frac{\epsilon_g^{(20)}}{2}\frac{\partial E_{m+2,n+N}}{\partial r}=0
\end{aligned}\tag{71}$$

$$\begin{aligned}
&\frac{\partial}{\partial r}r^3\left(\frac{\omega^2}{\bar{v}_A^2}-k_{m+2,n+N}^2\right)\frac{\partial E_{m+2,n+N}}{\partial r}+Q_{m+2,n+N}E_{m+2,n+N}\\
&+\frac{\partial}{\partial r}r^3\left(\frac{\omega^2}{\bar{v}_A^2}-k_{m,n}k_{m+2,n+N}\right)\frac{\epsilon_g^{(21)}}{2}\frac{\partial E_{m,n}}{\partial r}\\
&+\frac{\partial}{\partial r}r^3\left(\frac{\omega^2}{\bar{v}_A^2}-k_{m+2,n+N}k_{m,n+N}\right)\frac{\epsilon_g^{(20)}}{2}\frac{\partial E_{m,n+N}}{\partial r}=0
\end{aligned}\tag{72}$$

$$\begin{aligned}
&\frac{\partial}{\partial r}r^3\left(\frac{\omega^2}{\bar{v}_A^2}-k_{m-2,n}^2\right)\frac{\partial E_{m-2,n}}{\partial r}+Q_{m-2,n}E_{m-2,n}\\
&+\frac{\partial}{\partial r}r^3\left(\frac{\omega^2}{\bar{v}_A^2}-k_{m,n+N}k_{m-2,n}\right)\frac{\epsilon_g^{(21)}}{2}\frac{\partial E_{m,n+N}}{\partial r}\\
&+\frac{\partial}{\partial r}r^3\left(\frac{\omega^2}{\bar{v}_A^2}-k_{m-2,n}k_{m,n}\right)\frac{\epsilon_g^{(20)}}{2}\frac{\partial E_{m,n}}{\partial r}=0
\end{aligned}\tag{73}$$

The MAE gap determined by Eqs. (70)–(73) is shown in Fig. 10. In order to demonstrate the effect of coupling due to the helicity and ellipticity parameters, $\epsilon^{(21)}$ and $\epsilon^{(20)}$, the gaps obtained when both these parameters or one of them are neglected are also shown

in this figure. We observe that the interaction of the main modes, (m, n) and $(m, n+N)$, with the $(m-2, n)$ and $(m+2, n+N)$ satellites essentially affects the width and location of the MAE gap. On the other hand, comparing Fig. 10 with Fig. 4, we conclude that adding these satellites enables us to reproduce the actual width of the gap with sufficient accuracy, which justifies using Eqs. (70)–(73) in our calculations. Figure 11 demonstrates two examples of MAE modes with different mode numbers in the homogeneous plasma. Only the the main MAE components $[(m, n)$ and $(m, n+N)]$ are shown. Like in the case of HAE_{21}, we obtain a pair of eigenfunctions (with opposite and coinciding phases of the main components) for each set of mode numbers. Calculations carried out for inhomogeneous plasmas have shown that any realistic inhomegeneity kills MAEs of global character.

One can note that the asymptotic behavior of the obtained eigenfunctions at $r \to 0$ is oscillatory (the eigenfunctions change the sign with radial wavelength decreasing when $r \to 0$), which is especially well seen for the HAE_{21} eigenfunctions. This behavior, which never was observed for TAEs, is associated with the fact that the coupling parameters producing the eigenmodes studied here, $\epsilon^{(20)}$ and $\epsilon^{(21)}$, does not vanish at $r = 0$. To show this, we write the system of equations for two coupled harmonics, Eqs. (43), (44), in the matrix form:

$$\frac{d}{dr}\left(r^3 \mathcal{A} \frac{dE}{dr}\right) + r\mathcal{Q}E = 0, \tag{74}$$

where $E = \mathrm{col}(E_1, E_2)$ are the wave functions of the two coupled modes,

$$\mathcal{A} = \begin{pmatrix} a_{11} & \epsilon a_{12} \\ \epsilon a_{12} & a_{22} \end{pmatrix} = \mathcal{A}_{(0)} + \mathcal{A}_{(1)} r + \mathcal{A}_{(2)} r^2 + \ldots, \tag{75}$$

$$\mathcal{Q} = \begin{pmatrix} a_{11}(1 - m_1^2) & 0 \\ 0 & a_{22}(1 - m_2^2) \end{pmatrix} = \mathcal{Q}_{(0)} + \mathcal{Q}_{(1)} r + \mathcal{Q}_{(2)} r^2 + \ldots, \tag{76}$$

m_1 and m_2 are the poloidal wavenumbers of the modes. Looking for solutions in the form $E = r^\alpha \mathrm{col}(e_1, e_2)$, where $e_j = \sum_{j=0}^{\infty} e_{j(l)} r^l$, $j = 1, 2$, we obtain the following equation for α:

$$\left|\gamma A_{(0)} + \mathcal{Q}_{(0)}\right| = 0, \tag{77}$$

where $\gamma = \alpha(\alpha + 2)$.

When $\epsilon = 0$, Eq. (77) yields the asymptotics for the two equations considered independently:

$$\gamma = m_{1,2}^2 - 1, \quad \alpha = -1 \pm m_{1,2}. \tag{78}$$

In a general case, omitting terms of the order of ϵ^4, we obtain:

$$\gamma = \frac{s_1 + s_2}{2} + \epsilon_{(0)}^2 \frac{a_{12(0)}^2 (s_1 + s_2)}{2|\mathcal{A}_{(0)}|} \pm \frac{1}{2}\left[(s_1 - s_2)^2 + 2\epsilon_{(0)}^2 \frac{a_{12(0)}^2 (s_1^2 + s_2^2)}{|\mathcal{A}_{(0)}|}\right]^{1/2}, \tag{79}$$

$$\alpha = -1 \pm (1 + \gamma)^{1/2}, \tag{80}$$

where $s_{1,2} = m_{1,2}^2 - 1$. Now we recall that $|\mathcal{A}| = (\omega^2 - \omega_1^2)(\omega^2 - \omega_2^2)/\bar{v}_A^4$, where $\omega_{1,2}$ are the roots of the equation $|A| = 0$. Hence, $|\mathcal{A}_{(0)}| < 0$ when ω lies within the gap, and we conclude that γ and, thus, α become complex when the second (negative) term under the square root dominates. This means that the asymptotic of the wave function becomes oscillatory,

$$E \propto r^{\alpha_R} \exp[i\alpha_I \ln(r)], \tag{81}$$

where $\alpha_R = \mathrm{Re}(\alpha)$, $\alpha_I = \mathrm{Im}(\alpha)$.

In the considered cases of MAE and HAE_{21}, the width of the gaps weakly changes with the radius, whence $\epsilon_{(0)}^2/|\mathcal{A}_{(0)}|$ is of the order of unity, increasing near the tips of the gaps. In particular, in the case of MAE, the expression under the square root in Eq. (79) is always negative because $s_1 = s_2$. We conclude that eigenfunctions may well manifest oscillatory behavior in the considered cases, and the asymptotic behavior of the MAE eigenfunctions is always oscillatory. On the other hand, α is always real, and oscillatory asymptotics are not possible when $\epsilon \to 0$ at $r \to 0$.

Thus, the appearance of the oscillatory eigenfunctions indeed correlates with the oscillatory character of the asymptotic behavior of solutions of the considered equations. However, further studies are required to be certain that this phenomena are really connected and to understand the nature of the obtained oscillatory solutions.

VII. GLOBAL ALFVÉN EIGENMODES

We have shown above that the plasma inhomogeneity tends to make closed the gaps in the Alfvén continuum and, thus, tends to prevent the existence of eigenmodes of the global character (i.e., the modes with the perturbation covering almost the whole plasma cross section). On the other hand, the so-called "global Alfvén eigenmodes", GAEs, which are not associated with the gaps, can exist only in an inhomogeneous plasma. The GAEs exist even in the cylindrical geometry and have the frequencies close (just below) to the minimum of $\omega_A(r)$. The mentioned minimum is located at r_0 determined by the following equation:

$$\frac{n}{m} = \iota(r_0) + 2L_\rho(r_0)\iota'(r_0) \tag{82}$$

where $L_\rho = -(\rho'/\rho)^{-1}$, prime means the radial derivative. It follows from Eq. (82) that $\mathrm{sgn}(mn) > 0$ for $L_\rho > 0$ (which is normally the case) and $\iota' > 0$. The location of the minimum of $\omega_A(r)$ in a Helias reactor with the density profile given by Eq. (69) is shown in Fig. 12.

To study GAEs in a Helias reactor, we restrict ourselves to the cylindrical approximation, i.e., neglect all coupling parameters $\epsilon^{(\mu\nu)}$. Results of the numerical solution of Eq. (28) with low m, n in this approximation are shown in Figs. 13, 14. It follows from Figs. 13, 14 that there are discrete solutions, as one could expect. But, on the other hand, we observe that the continuum curve is rather flat, which is a consequence of the small shear and the rather flat profile shape of $n(r)$. This indicates that the magnetic well responsible for the existence of the eigenfunctions is rather shallow. Therefore, the solutions must be sensitive to the shear. To verify this, we have added the small terms neglected in Eq. (29), i.e., replaced $Q_{m,n}$ by $Q^{(1)}_{m,n}$,

$$Q^{(1)}_{m,n} = Q_{m,n} + \frac{k^2_{m,n} r^3}{\delta_0}\left(\frac{\omega^2}{\bar{v}^2_A} - k^2_{m,n}\right) - k_{m,n} r^2 (3k'_{m,n} + r k''_{m,n}). \tag{83}$$

We have found numerically that there are no GAE modes in this case. Thus, a question arises why it happens. The analysis below is aimed at answering this question.

First of all, we note that GAEs are really global (and justify their name) only when $m = n = 1$. When the wave numbers exceed unity, they become localized near r_0. We use this fact by assuming $m, n > 1$ and expanding ω_A to second order in $r - r_0$ (we follow the approach of Ref. [41]):

$$\omega_A^2 = \omega_{A0}^2 + (1/2)\left(\omega_A^2\right)_0'' (r - r_0)^2 \equiv \omega_{A0}^2 \left(1 + x^2/L^2\right) \tag{84}$$

where $L^2 \equiv 2\omega_{A0}^2/(\omega_A^2)_0''$, $x = r - r_0$, the subscript "0" indicates that a quantity is taken at r_0. Taking into account that x is small, we write an approximate equation for GAEs in the form

$$\frac{\partial}{\partial x} r_0^3 \frac{\omega_{A0}^2}{L^2 \bar{v}_{A0}^2} \left(x^2 + \Delta^2\right) \frac{\partial E_{m,n}}{\partial x} + \left[r \left(\frac{k_\parallel^2 r^2}{\delta} - m^2 + 1 \right) \frac{\omega_A^2}{L^2 \bar{v}_A^2} \left(x^2 + \Delta^2\right) - r^2 \left(\frac{\omega^2}{\bar{v}_A^2} \right)' + k_\parallel \left(3r^2 k_\parallel' + r^3 k_\parallel'' \right) \right] \Bigg|_{r=r_0} E_{m,n} = 0, \tag{85}$$

where $\Delta^2 = L^2(\omega_{A0}^2 - \omega^2)/\omega_{A0}^2 > 0$. To proceed further, we transform Eq. (85) to a Schrödinger-like equation by introducing a new wave function, $\Psi = \sqrt{F} E$, where $F = r_0^3 \left(\omega_{A0}/L^2 v_A\right)\left(x^2 + \Delta^2\right)$. Introducing the dimensionless variable $y = x/\Delta$, we obtain:

$$\Psi''(y) + [\mathcal{E} - V(y)]\,\Psi(y) = 0, \tag{86}$$

where

$$\mathcal{E} = \left(\frac{k_\parallel^2}{\delta_0} - \frac{m^2 - 1}{r_0^2} \right) \Delta^2, \quad V(y) = \frac{1}{(1 + y^2)^2} - \frac{b}{1 + y^2}, \quad b = \frac{L^2}{r_0 L_\rho} + \frac{L^2}{r_0} \frac{3\iota' + r_0 \iota''}{\iota - n/m}. \tag{87}$$

The constant $\mathcal{E}$ and the function $V(y)$ can be considered as the effective full energy and the effective potential energy, respectively. When $b \leq 0$, $V(y)$ has no minimum at finite y, which means that there is only a continuous spectrum. Discrete modes arise when $b > 0$: in this case there are two minima of $V(y)$ for $0 \leq b \leq 2$, $V(y)$ and one minimum for $b \geq 2$, $V(y)$.

Using Eq. (82), we transform b to the form:

$$b = -\frac{L^2}{2 L_\rho r_0} \left(1 + \frac{\iota'' r_0}{\iota'} \right) \tag{88}$$

It follows from Eq. (88) that a necessary condition for the existence of discrete spectrum is $\mathrm{sgn}(\iota' \iota'') < 0$. This condition is not satisfied for a Helias reactor, where $\iota' > 0$, whereas

$\iota'' < 0$. On the other hand, if the shear terms are neglected in Eq. (83), $b = L^2/(r_0 L_\rho) > 0$, and, thus, discrete modes exist. This explains the different results obtained numerically when $Q_{m,n}$ was replaced by $Q^{(1)}_{m,n}$.

As mentioned in Sec. II, the metric tensor was derived in the assumption that the shear is of the order of r^2/R_0^2. Then the shear term in the equation for AEs is of higher order. This implies that GAEs are likely to exist in the Helias configuration. However, further investigation is required for a reliable conclusion. Note that such a problem does not arise in tokamaks because the shear term is absent when the rotational transform is produced by the plasma current (it is canceled by the term associated with the current).

VIII. SUMMARY AND CONCLUSIONS

In this work, we derived an equation of shear Alfvén waves in Helias configurations, which describes all kinds of shear Alfvén eigenmodes in the framework of ideal MHD. The metric tensor components entering this equation were found analytically by means of the expansion of the equilibrium magnetic field in the vicinity of the magnetic axis. Further work in this direction is required to find more exact expressions for the metric tensor, which will provide a possibility to study the whole family of AE modes in Helias systems. Two numerical codes were developed. One of them, COBRA, calculates the structure of the Alfvén continuum in Helias configurations. Another one, BOA, solves the set of equations for AEs, giving eigenfrequencies and eigenfunctions (radial structure) of Alfvén perturbations.

The results of investigation of AEs carried out with the use of the mentioned codes and analytically can be summarized as follows.

We have found that the presence of several dominant harmonics in the Fourier spectrum of the magnetic field strength results in the MAE, HAE_{11}, and TAE gaps. In addition, we have found that the variation of the plasma cross section shape along the large azimuth of the torus is an important factor affecting the Alfvén frequency spectrum. It strongly contributes to the MAE gap and leads to coupling of the modes with other

mode numbers than those determined by Fourier harmonics in B_0. In particular, it leads to the HAE_{21}, HAE_{22}, and EAE gaps. Especially large is the HAE_{21} gap associated with the rotation of the non-circular plasma cross section. The large magnitudes of coupling parameters, first of all, $\epsilon^{(21)}$, results in appearance of rather essential secondary and higher-order gaps in the vicinity of the frequency determined by $|k_{m,n}|v_A(r_*) = |k_{m+\mu,n+\nu N}|v_A(r_*)$ formed due to interaction of more than two waves when direct interaction between the modes with the numbers m, n and $m+\mu, n+\nu N$ is not possible (i.e., when $\epsilon^{(\mu\nu)} = 0$). Furthermore, large magnitude of the coupling parameters significantly affects the gaps arising due to direct interaction of two waves; namely it displaces the gaps and changes their width. These effects were investigated analytically and numerically by means of the code COBRA. As a result, the Alfvén continuum structure in a Helias configuration relevant to W7-X and a Helias reactor was obtained.

Using the code BOA, we have shown that there exist discrete HAE_{21} and MAE modes due to coupling of the modes with m, $n \leftrightarrow m+2$, $n+N$ and m, $n \leftrightarrow m$, $n+N$, respectively. MAEs were obtained by solving a set of equations consisting of four equations to take into account the multiple-wave interaction, which is essential in this case. It was found that the radial structure and even the existence of HAE_{21} modes and, especially, MAEs depend on the radial profile shape of the plasma density. In particular, it was found that global eigenmodes, i.e., perturbations covering the whole plasma cross section or the large part of it, disappear when the plasma density at the edge is sufficiently small.

Both HAE_{21} and MAE modes belong to the high-frequency part of shear Alfvén spectrum. They are characterized by such longitudinal wave numbers that they can interact with circulating alpha particles having the energy $\mathcal{E} > 1\,\mathrm{MeV}$ in high-β plasmas of a Helias reactor (note that the fraction of circulating particles in Heliases is much greater than that in tokamaks because of the difference in the aspect ratio of these systems; therefore, circulating particles constitute a vast majority of energetic alphas in a Helias reactor). In contrast to this, TAE modes can hardly interact with these particles. In order to see it, we allow for the fact that circulating α-particles interact with Alfvén waves mainly through the resonance $\omega - (k_\parallel \pm \iota/R_0)v_\parallel = 0$, where $v_\parallel$ is the particle velocity along the

magnetic field. It follows from the resonance condition that a particle interacts with the waves provided that its parallel velocity is

$$v_{\|}^{res} = v_A \left(1 \mp \frac{2\iota_*}{N\nu - \mu\iota_*}\right)^{-1}. \tag{89}$$

The magnitude of $v_{\|}^{res}$ determined by Eq. (89) depends on the kind of AEs. In particular, $|v_{\|}^{res}/v_A| = 1$ or $1/3$ for TAEs; when $N = 5$, $\iota = 0.9$, Eq. (89) yields $v_{\|}^{res}/v_A = 1.56$ and 0.64 for MAE modes, $v_{\|}^{res}/v_A = 2.28$ and 0.64 for HAE_{21} modes. Therefore, the particles with $v_{\|} > v_A$ can be in the resonance with MAE and HAE_{21} modes. On the other hand, $v_\alpha^2/v_A^2 = \beta M_i \mathcal{E}/(2M_\alpha T)$, where v_α is the alpha velocity, T is the plasma temperature, M_α and M_i are the masses of an α-particle and a background ion (M_i should be taken to be equal to 2.5 deuteron mass for a 50-50% deuterium-tritium plasma), respectively. We obtain from here that $v_\alpha/v_A = 1.8 \div 3.3$ for α-particles with $\mathcal{E} = 1 \div 3.5\,\mathrm{MeV}$ in the Helias reactor with $T(0) = 15\,\mathrm{keV}$, $\beta(0) = 15\%$ [25]. Thus, due to Eq. (89), the resonant pitch angles of these particles, $\chi^{res} \equiv v_{\|}^{res}/v_\alpha$, lie in the range $0.5 \lesssim \chi^{res} \lesssim 0.9$ for MAEs and $0.7 \lesssim \chi^{res} \leq 1$ for HAE_{21}. The obtained magnitudes of the pitch angles are relevant to circulating particles, as one can see from the condition $\chi^{circ} > \sqrt{A^{-1} r/a}$, where $A \approx 10$ is the aspect ratio of the torus. Therefore, we conclude that both HAE_{21} and MAE modes (but not TAE modes) can interact with $1 \div 3.5\,\mathrm{MeV}$ circulating alphas in the plasma core. Note that the considered AEs can also play an important role in W7-X, where the energetic ions will be produced during neutral beam injection and have the velocity less than Alfvén velocity.

In addition to the eigenmodes residing in the continuum gaps, the GAE modes are considered. It has been found that the magnetic well responsible for their existence is rather shallow when the magnetic shear is small and the plasma density profile is flat. This requires especially accurate analysis to make reliable predictions concerning GAEs in Helias configurations.

ACKNOWLEDGEMENTS

The work is carried out within the Partner Project Agreement No. P-034 between the Science and Technology Center in Ukraine and the Scientific Center "Institute for Nuclear Research", and Max-Planck-Institut für Plasmaphysik. The authors thank A. Weller for a discussion. One of the authors (Ya.K.) would like to acknowledge the hospitality of the Max-Planck-Institut für Plasmaphysik.

APPENDIX A: METRIC TENSOR OF THE FLUX COORDINATE SYSTEM

The aim of the calculations presented in this appendix is to derive analytically the metric tensor of the Boozer flux coordinates in a general stellarator configuration. The derivation employs the near-axis expansion of the plasma equilibrium suggested in Ref. [43], where it was used to analyze the Fourier spectrum of the magnetic field strength. The expansion uses the average radius of a flux surface (or, more exactly, the ratio of it to the other characteristic lengths, first of all, to the curvature radius of the magnetic axis) as a small parameter. An advantage of the expansion is its simplicity, but its serious disadvantage is that one has to get to the second order in order to study any effects of the magnetic shear. However, this shortcoming does not seem serious when we are interested in weak-shear configurations like Wendelstein 7-X or the Helias Reactor.

Following Ref. [43], we write the spatial position of a point, $\vec{r}$, as a function of the flux coordinates (ψ, θ, ϕ):

$$\vec{r}(\psi,\theta,\phi) = \vec{r}_0(\phi) + X(\psi,\theta,\phi)\hat{\vec{\kappa}}(\phi) + Y(\psi,\theta,\phi)\hat{\vec{b}}(\phi) + Z(\psi,\theta,\phi)\hat{\vec{\tau}}(\phi), \qquad \text{(A1)}$$

where ψ is a flux surface label (the toroidal magnetic flux enclosed in a flux surface); θ and ϕ are specially chosen poloidal and toroidal angular coordinates; $\vec{r}_0(\phi)$ is the spatial position of the magnetic axis; $\hat{\vec{\tau}}(\phi)$, $\hat{\vec{\kappa}}(\phi)$, and $\hat{\vec{b}}(\phi)$ are the tangent, normal, and binormal (the Frenet unit vectors) of the magnetic axis, respectively. The unknown functions $X(\psi,\theta,\phi)$, $Y(\psi,\theta,\phi)$, and $Z(\psi,\theta,\phi)$ are assumed to satisfy the condition $X(\psi = 0) = Y(\psi = 0) = Z(\psi = 0) = 0$. Then they are presented as power series in $\varepsilon \equiv \psi^{1/2}$,

$$X(\psi,\theta,\phi) = \varepsilon X_{(1)}(\theta,\phi) + \varepsilon^2 X_{(2)}(\theta,\phi) + \varepsilon^3 X_{(3)}(\theta,\phi) + \ldots, \tag{A2}$$

and the same for $Y(\psi,\theta,\phi)$ and $Z(\psi,\theta,\phi)$. Note that the coefficient numbers in all power expansions in ε is denoted within this Appendix as subscripts enclosed in parentheses to avoid confusion with numbers of Fourier harmonics etc. If the function $\psi(\vec{x})$ is analytic, as well as $\theta(\vec{x})$ and $\phi(\vec{x})$ aside from $\psi = 0$, the Fourier series of $X_{(1)}(\theta,\phi)$, $Y_{(1)}(\theta,\phi)$, and $Z_{(1)}(\theta,\phi)$ in θ can contain only first harmonics,

$$X_{(1)}(\theta,\phi) = X_{(1)s}(\phi)\sin(\theta) + X_{(1)c}(\phi)\cos(\theta); \tag{A3}$$

those of $X_{(2)}(\theta,\phi)$, $Y_{(2)}(\theta,\phi)$, and $Z_{(2)}(\theta,\phi)$, zeroth and second harmonics; those of $X_{(3)}(\theta,\phi)$, $Y_{(3)}(\theta,\phi)$, and $Z_{(3)}(\theta,\phi)$, first and third harmonics; those of $X_{(4)}(\theta,\phi)$, $Y_{(4)}(\theta,\phi)$, and $Z_{(4)}(\theta,\phi)$, zeroth, second, and fourth harmonics; etc. [43]

Expressions for the covariant base vectors $\vec{e}_\psi \equiv \partial\vec{r}/\partial\psi$, $\vec{e}_\theta \equiv \partial\vec{r}/\partial\theta$, and $\vec{e}_\phi \equiv \partial\vec{r}/\partial\phi$ can be obtained by differentiating Eq. (A1):

$$\vec{e}_\psi = \frac{1}{2\varepsilon}\left(\frac{\partial X}{\partial\varepsilon}\hat{\vec{\kappa}} + \frac{\partial Y}{\partial\varepsilon}\hat{\vec{b}} + \frac{\partial Z}{\partial\varepsilon}\hat{\vec{\tau}}\right), \tag{A4}$$

$$\vec{e}_\theta = \frac{\partial X}{\partial\theta}\hat{\vec{\kappa}} + \frac{\partial Y}{\partial\theta}\hat{\vec{b}} + \frac{\partial Z}{\partial\theta}\hat{\vec{\tau}}, \tag{A5}$$

$$\begin{aligned}\vec{e}_\phi = &\left(\frac{\partial X}{\partial\phi} + Y\tau\frac{dl}{d\phi} + Z\mathcal{K}\frac{dl}{d\phi}\right)\hat{\vec{\kappa}} + \left(\frac{\partial Y}{\partial\phi} - X\tau\frac{dl}{d\phi}\right)\hat{\vec{b}} \\ &+ \left(\frac{\partial Z}{\partial\phi} + \frac{dl}{d\phi} - X\mathcal{K}\frac{dl}{d\phi}\right)\hat{\vec{\tau}},\end{aligned} \tag{A6}$$

where $l(\phi)$ is the distance along the magnetic axis, $dl/d\phi = |d\vec{r}_0/d\phi|$, $\mathcal{K} = \mathcal{K}(\phi)$ and $\tau = \tau(\phi)$ are the curvature and torsion of the magnetic axis, and the Frenet formulae [44] have been used to find the ϕ derivatives of the Frenet unit vectors. Note that $\mathcal{K}$ here denotes the curvature of the magnetic axis rather than the curvature of magnetic field lines, as in the main part of the work, but this usage will not lead to a confusion since we will not be interested in the curvature of magnetic field lines within this appendix.

In Boozer coordinates the magnetic field, $\vec{B}$, can be written in the two following forms (the covariant and contravariant ones):

$$\vec{B} = \frac{\iota(\psi)}{\sqrt{g}}\vec{e}_\theta + \frac{1}{\sqrt{g}}\vec{e}_\phi$$
$$= B_\psi(\psi,\theta,\phi)\vec{e}^{\,\psi} + B_\theta(\psi)\vec{e}^{\,\theta} + B_\phi(\psi)\vec{e}^{\,\phi}. \tag{A7}$$

Here

$$\sqrt{g} = [B_\phi(\psi) + \iota(\psi)B_\theta(\psi)]B^{-2}(\psi,\theta,\phi) \tag{A8}$$

is the determinant of the metric tensor; $\vec{e}^{\,\psi} \equiv \nabla\psi$, $\vec{e}^{\,\theta} \equiv \nabla\theta$, and $\vec{e}^{\,\phi} \equiv \nabla\phi$ are the contravariant base vectors of the coordinate system; $\iota(\psi)$ is the rotational transform; $B_\theta(\psi)$ and $B_\phi(\psi)$ are, in fact, the toroidal current inside a flux surface and the poloidal current outside it (up to a constant factor); the B_ψ term is the contribution of generalized Pfirsch-Schlüter currents (it vanishes in the absence of the pressure gradient, ∇p).

The equilibrium equation, $\nabla p = \vec{j}\times\vec{B}/c$, is reduced in the Boozer coordinates to the combination of the equation of the flux-surface-averaged pressure balance,

$$\frac{dB_\phi}{d\psi} + \frac{dB_\theta}{d\psi} + 4\pi\frac{dp}{d\psi}\frac{B_\phi + \iota B_\theta}{\langle B^2\rangle} = 0, \tag{A9}$$

where

$$\langle B^2\rangle = \frac{\oint d\phi \oint d\theta\sqrt{g}B^2}{\oint d\phi \oint d\theta\sqrt{g}} = \frac{4\pi^2}{\oint d\phi \oint d\theta B^{-2}} \tag{A10}$$

is the average of B^2 on a magnetic surface, and a relation between B_ψ and $dp/d\psi$,

$$\frac{\partial B_\psi}{\partial\phi} + \iota\frac{\partial B_\psi}{\partial\theta} = \left(\frac{\langle B^2\rangle}{B^2} - 1\right)\frac{4\pi(B_\phi + \iota B_\theta)}{\langle B^2\rangle}\frac{dp}{d\psi}, \tag{A11}$$

which enables us to determine the Fourier spectrum of B_ψ in terms of that of B^{-2}. Namely, if

$$\frac{1}{B^2(\psi,\theta,\phi)} = \frac{1}{\langle B^2\rangle}$$
$$\times\left\{1 + \sum_{|m|+|n|\neq 0}[\lambda_{mnc}(\psi)\cos(n\phi - m\theta) + \lambda_{mns}(\psi)\sin(n\phi - m\theta)]\right\} \tag{A12}$$

then

$$B_\psi(\psi,\theta,\phi) = 4\pi\frac{dp}{d\psi}\frac{B_\phi + \iota B_\theta}{\langle B^2\rangle}\sum_{|m|+|n|\neq 0}\frac{1}{n - \iota m}[\lambda_{mnc}(\psi)\sin(n\phi - m\theta)$$
$$- \lambda_{mns}(\psi)\cos(n\phi - m\theta)]. \tag{A13}$$

It is assumed that

$$B^{-2}(\psi,\theta,\phi) = (B^{-2})_{(0)}(\phi) + (B^{-2})_{(1)}(\theta,\phi)\varepsilon + (B^{-2})_{(2)}(\theta,\phi)\varepsilon^2 + \ldots, \tag{A14}$$

$$B_\psi(\psi,\theta,\phi) = B_{\psi(0)}(\phi) + B_{\psi(1)}(\theta,\phi)\varepsilon + B_{\psi(2)}(\theta,\phi)\varepsilon^2 + \ldots, \tag{A15}$$

$$\iota(\psi) = \iota_{(0)} + \iota_{(2)}\varepsilon^2 + \iota_{(4)}\varepsilon^4 + \ldots, \tag{A16}$$

$$B_\phi(\psi) = B_{\phi(0)} + B_{\phi(2)}\varepsilon^2 + B_{\phi(4)}\varepsilon^4 + \ldots, \tag{A17}$$

$$B_\theta(\psi) = B_{\theta(2)}\varepsilon^2 + B_{\theta(4)}\varepsilon^4 + \ldots, \tag{A18}$$

with the Fourier spectra of $(B^{-2})_{(i)}(\theta,\phi)$ and $B_{\psi(i)}(\theta,\phi)$ obeying the same rules as those of $X_{(i)}(\theta,\phi)$.

The procedure of calculating the parameters of equilibrium proposed by Garren and Boozer [43] is as follows. Equations (A9), (A12), (A13), and the equation

$$\vec{\Xi} \equiv \iota\vec{e}_\theta + \vec{e}_\phi - B_\psi\vec{e}_\theta\times\vec{e}_\phi - B_\theta\vec{e}_\phi\times\vec{e}_\psi - B_\phi\vec{e}_\psi\times\vec{e}_\theta = 0, \tag{A19}$$

which is just another form of Eq. (A7), are expanded in powers of ε and analyzed order by order. Another useful equation, which also follows from Eq. (A7) and provides a convenient way to find $B(\psi,\theta,\phi)$, is

$$B^{-2}(\psi,\theta,\phi) = \frac{|\vec{e}_\phi + \iota\vec{e}_\theta|^2}{(B_\phi + \iota B_\theta)^2}. \tag{A20}$$

We have found it convenient to organize the calculations as follows. First, it turns out that the equation $(X_{(1)}\hat{\vec{\kappa}} + Y_{(1)}\hat{\vec{b}})\cdot\vec{\Xi}_{(i)} = 0$ enables one to express $Z_{(i+1)}$ in terms of $X_{(i)}$ and $Y_{(i)}$. The obtained expression is substituted for $Z_{(i+1)}$ in the equation $(Y_{(1)}\hat{\vec{\kappa}} - X_{(1)}\hat{\vec{b}})\cdot\vec{\Xi}_{(i)} = 0$. The obtained equation for of $X_{(i)}$ and $Y_{(i)}$ is analyzed together with $\hat{\vec{\tau}}\cdot\vec{\Xi}_{(i-1)} = 0$. When doing this, relations obtained by expanding Eqs. (A9), (A12), and (A13) are used as required. We proceed to performing this procedure.

The ε^0 order of Eq. (A20) yields:

$$\frac{dl}{d\phi} = \frac{B_{\phi(0)}}{B_{(0)}(\phi)}, \tag{A21}$$

which enables us to relate $B_{\phi(0)}$ and the length of the magnetic axis, L: $L = B_{\phi(0)} \oint d\phi\, B_{(0)}^{-1}(\phi)$. Using Eq. (A21), we can transform the equation $\hat{\vec{\tau}} \cdot \vec{\Xi}_{(0)} = 0$ to the form

$$X_{(1)} \frac{\partial Y_{(1)}}{\partial \theta} - Y_{(1)} \frac{X_{(1)}}{\partial \theta} = \frac{2}{B_{(0)}}, \tag{A22}$$

which is a mathematical expression of the fact that the square of a flux surface depends on ϕ as B^{-1}. Finally, it follows from the equation $(X_{(1)}\hat{\vec{\kappa}} + Y_{(1)}\hat{\vec{b}}) \cdot \vec{\Xi}_{(0)} = 0$ that $Z_{(1)} = 0$ and, thus, $Z = \mathcal{O}(\varepsilon^2)$.

Then we consider the first-order equation $(X_{(1)}\hat{\vec{\kappa}} + Y_{(1)}\hat{\vec{b}}) \cdot \vec{\Xi}_{(1)} = 0$, which yields:

$$Z_{(2)} = -\frac{B_{(0)}}{4B_{\phi(0)}} \left[\frac{\partial}{\partial \phi}(X_{(1)}^2 + Y_{(1)}^2) + \iota_{(0)} \frac{\partial}{\partial \theta}(X_{(1)}^2 + Y_{(1)}^2) \right] + \frac{B_{\psi(0)}}{B_{(0)}}. \tag{A23}$$

To proceed further, we need to specify the dependence of $X_{(1)}$ and $Y_{(1)}$ on θ. As mentioned above, both are linear combinations of $\sin(\theta)$ and $\cos(\theta)$ [cf. Eq. (A3)]. We take them in the following form satisfying Eq. (A22):

$$\begin{aligned} X_{(1)} = \left(\frac{2}{B_{(0)}(\phi)} \right)^{1/2} & \{ \kappa^{1/2}(\phi) \cos[\gamma(\phi)] \cos[\theta - \theta_0(\phi)] \\ & - \kappa^{-1/2}(\phi) \sin[\gamma(\phi)] \sin[\theta - \theta_0(\phi)] \}, \end{aligned} \tag{A24}$$

$$\begin{aligned} Y_{(1)} = \left(\frac{2}{B_{(0)}(\phi)} \right)^{1/2} & \{ \kappa^{1/2}(\phi) \sin[\gamma(\phi)] \cos[\theta - \theta_0(\phi)] \\ & + \kappa^{-1/2}(\phi) \cos[\gamma(\phi)] \sin[\theta - \theta_0(\phi)] \}. \end{aligned} \tag{A25}$$

Equations (A24), (A25) include three parameters: $\kappa(\phi)$, the elongation of the cross section, $\theta_0(\phi)$, the poloidal angle of one of the main axes of the ellipse, and $\gamma(\phi)$, the angle between the ellipse axis and the normal to the magnetic axis.

Substituting Z_2, X_1, and Y_1 given by Eqs. (A23)–(A25) into the equation $(X_{(1)}\hat{\vec{\kappa}} + Y_{(1)}\hat{\vec{b}}) \cdot \vec{\Xi}_{(1)} = 0$, we arrive after some algebra at the following equation for the rotational transform:

$$\iota_{(0)} = \frac{d\theta_0}{d\phi} + \frac{2}{\kappa(\phi) + \kappa^{-1}(\phi)} \left[\frac{d\gamma}{d\phi} - \frac{B_{\phi(0)}}{B_{(0)}(\phi)} \left(\tau(\phi) + \frac{B_{\theta(2)}}{2} \right) \right]. \tag{A26}$$

Now we can calculate the components of the covariant and contravariant metric tensors to the lowest order. Using Eqs. (A4)–(A6), we obtain the components of the covariant metric tensor $g_{ij} = \vec{e}_i \cdot \vec{e}_j$, where $i, j = \psi, \theta, \phi$:

$$g_{\psi\psi} = \frac{1}{4\varepsilon^2}\left[\left(\frac{\partial X}{\partial \varepsilon}\right)^2 + \left(\frac{\partial Y}{\partial \varepsilon}\right)^2 + \left(\frac{\partial Z}{\partial \varepsilon}\right)^2\right] = \mathcal{O}(\varepsilon^{-2}), \tag{A27}$$

$$g_{\psi\theta} = g_{\theta\psi} = \frac{1}{2\varepsilon}\left(\frac{\partial X}{\partial \varepsilon}\frac{\partial X}{\partial \theta} + \frac{\partial Y}{\partial \varepsilon}\frac{\partial Y}{\partial \theta} + \frac{\partial Z}{\partial \varepsilon}\frac{\partial Z}{\partial \theta}\right) = \mathcal{O}(\varepsilon^0), \tag{A28}$$

$$\begin{aligned} g_{\psi\phi} = g_{\phi\psi} = \frac{1}{2\varepsilon}\Bigg[&\frac{\partial X}{\partial \varepsilon}\left(\frac{\partial X}{\partial \phi} + Y\tau\frac{B_{\phi(0)}}{B_{(0)}} + Z\mathcal{K}\frac{B_{\phi(0)}}{B_{(0)}}\right) \\ &+ \frac{\partial Y}{\partial \varepsilon}\left(\frac{\partial Y}{\partial \phi} - X\tau\frac{B_{\phi(0)}}{B_{(0)}}\right) \\ &+ \frac{\partial Z}{\partial \varepsilon}\left(\frac{\partial Z}{\partial \phi} + \frac{B_{\phi(0)}}{B_{(0)}} - X\mathcal{K}\frac{B_{\phi(0)}}{B_{(0)}}\right)\Bigg] = \mathcal{O}(\varepsilon^0), \end{aligned} \tag{A29}$$

$$g_{\theta\theta} = \left(\frac{\partial X}{\partial \theta}\right)^2 + \left(\frac{\partial Y}{\partial \theta}\right)^2 + \left(\frac{\partial Z}{\partial \theta}\right)^2 = \mathcal{O}(\varepsilon^2), \tag{A30}$$

$$\begin{aligned} g_{\theta\phi} = g_{\phi\theta} = &\frac{\partial X}{\partial \theta}\left(\frac{\partial X}{\partial \phi} + Y\tau\frac{B_{\phi(0)}}{B_{(0)}} + Z\mathcal{K}\frac{B_{\phi(0)}}{B_{(0)}}\right) \\ &+ \frac{\partial Y}{\partial \theta}\left(\frac{\partial Y}{\partial \phi} - X\tau\frac{B_{\phi(0)}}{B_{(0)}}\right) \\ &+ \frac{\partial Z}{\partial \theta}\left(\frac{\partial Z}{\partial \phi} + \frac{B_{\phi(0)}}{B_{(0)}} - X\mathcal{K}\frac{B_{\phi(0)}}{B_{(0)}}\right) = \mathcal{O}(\varepsilon^2), \end{aligned} \tag{A31}$$

$$\begin{aligned} g_{\phi\phi} = &\left(\frac{\partial X}{\partial \phi} + Y\tau\frac{B_{\phi(0)}}{B_{(0)}} + Z\mathcal{K}\frac{B_{\phi(0)}}{B_{(0)}}\right)^2 \\ &+ \left(\frac{\partial Y}{\partial \phi} - X\tau\frac{B_{\phi(0)}}{B_{(0)}}\right)^2 \\ &+ \left(\frac{\partial Z}{\partial \phi} + \frac{B_{\phi(0)}}{B_{(0)}} - X\mathcal{K}\frac{B_{\phi(0)}}{B_{(0)}}\right)^2 = \mathcal{O}(\varepsilon^0), \end{aligned} \tag{A32}$$

where we have taken into account that $X = \mathcal{O}(\varepsilon)$, $Y = \mathcal{O}(\varepsilon)$, $Z = \mathcal{O}(\varepsilon^2)$.

The components of the contravariant metric tensor, $g^{ij} = \vec{e}^{\,i} \cdot \vec{e}^{\,j}$, where $i, j = \psi, \theta, \phi$, can be expressed in terms of components of g_{ij} by means of the relation $g^{ij} = G^{ij}/g$,

where G^{ij} are the corresponding minors of the matrix g_{ij}. Using Eqs. (A8), (A27)–(A32), we find:

$$g^{\psi\psi} = \frac{g_{\theta\theta}g_{\phi\phi} - g_{\theta\phi}^2}{g} = B_{(0)}^2 g_{\theta\theta(2)}\varepsilon^2 + \mathcal{O}(\varepsilon^3), \tag{A33}$$

$$g^{\psi\theta} = g^{\theta\psi} = \frac{g_{\theta\phi}g_{\psi\phi} - g_{\psi\theta}g_{\phi\phi}}{g} = -B_{(0)}^2 g_{\psi\theta(0)} + \mathcal{O}(\varepsilon), \tag{A34}$$

$$g^{\psi\phi} = g^{\phi\psi} = \frac{g_{\psi\theta}g_{\theta\phi} - g_{\psi\phi}g_{\theta\theta}}{g} = \frac{B_{(0)}^4}{B_{\phi(0)}^2}(g_{\psi\theta(0)}g_{\theta\phi(2)} - g_{\psi\phi(0)}g_{\theta\theta(2)}) + \mathcal{O}(\varepsilon^3), \tag{A35}$$

$$g^{\theta\theta} = \frac{g_{\psi\psi}g_{\phi\phi} - g_{\psi\phi}^2}{g} = B_{(0)}^2 g_{\psi\psi(-2)}\varepsilon^{-2} + \mathcal{O}(\varepsilon^{-1}), \tag{A36}$$

$$g^{\theta\phi} = g^{\phi\theta} = \frac{g_{\psi\theta}g_{\psi\phi} - g_{\psi\psi}g_{\theta\phi}}{g} = \frac{B_{(0)}^4}{B_{\phi(0)}^2}(g_{\psi\theta(0)}g_{\psi\phi(0)} - g_{\psi\psi(-2)}g_{\theta\phi(2)}) + \mathcal{O}(\varepsilon), \tag{A37}$$

$$g^{\phi\phi} = \frac{g_{\psi\psi}g_{\theta\theta} - g_{\psi\theta}^2}{g} = \frac{B_{(0)}^4}{B_{\phi(0)}^2}(g_{\psi\psi(-2)}g_{\theta\theta(2)} - g_{\psi\theta(0)}^2) + \mathcal{O}(\varepsilon). \tag{A38}$$

Finally, we substitute the expressions given by Eqs. (A23)–(A25) for $Z_{(2)}$, $X_{(1)}$, and $Y_{(1)}$ in Eqs. (A27)–(A38) and use Eq. (A26) to exclude τ. After straightforward calculations (which, however, are rather cumbersome for the $g^{\psi\phi}$ and $g^{\theta\phi}$ components) we obtain the lowest-order approximations of the metric tensor components:

$$g^{\psi\psi} = 2B_{(0)}(\phi)\mathcal{P}[\theta, \phi, \kappa(\phi)]\varepsilon^2 + \mathcal{O}(\varepsilon^3), \tag{A39}$$

$$g^{\psi\theta} = g^{\theta\psi} = B_{(0)}(\phi)\mathcal{Q}(\theta, \phi) + \mathcal{O}(\varepsilon), \tag{A40}$$

$$g^{\psi\phi} = g^{\phi\psi} = -\frac{B_{(0)}(\phi)}{B_{\phi(0)}}\left\{B_{\theta(2)}\mathcal{Q}(\theta, \phi) + B_{\psi(0)}\mathcal{P}[\theta, \phi, \kappa^{-1}(\phi)]\right\}\varepsilon^2 + \mathcal{O}(\varepsilon^3), \tag{A41}$$

$$g^{\theta\theta} = \frac{B_{(0)}(\phi)}{2}\mathcal{P}[\theta, \phi, \kappa(\phi)]\varepsilon^{-2} + \mathcal{O}(\varepsilon^{-1}), \tag{A42}$$

$$\begin{aligned} g^{\theta\phi} = g^{\phi\theta} = \frac{B_{(0)}(\phi)}{B_{\phi(0)}}\Bigg\{&\frac{B_{(0)}(\phi)}{B_{\phi(0)}}\iota_{(0)} - B_{\psi(0)}\mathcal{Q}(\theta, \phi) \\ &- \frac{B_{\theta(2)}}{2}\mathcal{P}[\theta, \phi, \kappa(\phi)]\Bigg\} + \mathcal{O}(\varepsilon), \end{aligned} \tag{A43}$$

$$g^{\phi\phi} = \frac{B_{(0)}^2(\phi)}{B_{\phi(0)}^2} + \mathcal{O}(\varepsilon), \tag{A44}$$

where

$$\mathcal{P}(\theta, \phi, \kappa) = \frac{\kappa + \kappa^{-1}}{2} + \frac{\kappa - \kappa^{-1}}{2} \cos[2\theta - 2\theta_0(\phi)], \tag{A45}$$

$$\mathcal{Q}(\theta, \phi) = \frac{\kappa(\phi) - \kappa^{-1}(\phi)}{2} \sin[2\theta - 2\theta_0(\phi)]. \tag{A46}$$

The physics of the form of $g^{\psi\psi}$ given by Eq. (A39) is clear. In the absence of ellipticity, when $\mathcal{P} = 1$,

$$g^{\psi\psi} = 2B_{(0)}(\phi)\psi \tag{A47}$$

(at leading order), which is a mathematical expression of the conservation of the toroidal magnetic flux inside a flux surface. Indeed, if the radial dependence of the magnetic field is weak then the radius of a flux surface, $r(\phi)$, is associated with ψ by the equation $\psi = B_{(0)}(\phi)r^2(\phi)/2$. This is sufficient to reproduce Eq. (A47):

$$g^{\psi\psi} = |\nabla\psi|^2 = \left(\frac{d\psi}{dr}\right)^2 = B_{(0)}^2 r^2. \tag{A48}$$

Therefore, one can expect that Eq. (A39) correctly represents the modulation of $g^{\psi\psi}$ associated with the linked-mirror harmonic of the magnetic field ($m = 0$, $n = 5$) in the whole plasma cross section, at least, for not too large β, when the radial dependence of the linked-mirror harmonic is weak.

It is worth noting that the ordering of the metric tensor components in ε given by Eqs. (A39)–(A44) characterizes their asymptotic behavior at $\psi \to 0$ rather than the relative magnitude of the corresponding terms of Eq. (22). The reason is that the expansion parameter used within this appendix is the ratio of *the local radial coordinate* to the major radius of the device. In the main part of the work, we assume that unknown functions can undergo variations of the order of unity over the cross section. Therefore, we use as a small parameter the inverse aspect ratio understood as the ratio of *the characteristic cross-section radius*, r_{ch}, to the major radius. This is the same as long as we deal only

with equilibrium (one can find that terms of different order in ε appearing in the same component of the metric tensor always differ by a factor like $\mathcal{K}$, τ, B/B_ϕ, etc.). However, to estimate the contribution of the components to Eq. (22), we should find their order of magnitude, assuming that $r \sim (2\psi/B_{(0)})^{1/2} \sim r_{ch}$. Assuming also that $\beta \sim r_{ch}^2/R_0^2$ and having in mind Eqs. (A13) and (A26), we conclude that

$$B_{\theta(2)} \sim \frac{B_{(0)}}{G_{(0)}} \sim \frac{1}{R_0}, \tag{A49}$$

$$B_{\psi(0)} \sim \frac{d\beta}{dr}\frac{R_0}{r_{ch}} \sim \frac{1}{R_0}. \tag{A50}$$

Then Eqs. (A39)–(A44) yield the following order-of-magnitude estimates:

$$g^{\psi\psi} \sim B^2 r_{ch}^2, \quad g^{\psi\theta} \sim B, \quad g^{\theta\theta} \sim r_{ch}^{-2}, \tag{A51}$$

$$g^{\psi\phi} \sim \frac{B r_{ch}^2}{R_0^2}, \quad g^{\theta\phi} \sim \frac{1}{R_0^2}, \quad g^{\phi\phi} \sim \frac{1}{R_0^2}. \tag{A52}$$

Proceeding with the calculations, we can find next-order corrections to the metric tensor, which take account of the Shafranov shift and are necessary for correct treatment of TAE modes and HAE modes associated with the $m = 1$, $n = 5$ harmonic of the equilibrium magnetic field. Results of these calculations will be presented in the second part of this work.

APPENDIX B: SUBSTANTIATION OF THE EQUATION FOR THE CONTINUOUS SHEAR-ALFVÉN SPECTRUM.

It was shown in Ref. [45] that the continuous spectrum of the system

$$\mathcal{A}v = \mathcal{B}w, \quad \frac{\partial w}{\partial \psi} = \mathcal{C}v + \mathcal{D}w, \tag{B1}$$

where $\mathcal{A}$, $\mathcal{B}$, $\mathcal{C}$, $\mathcal{D}$ are linear differential operators *within* the flux surfaces (i.e., the derivatives are in directions within the flux surfaces), which depend linearly on λ, v and w are vectors describing the state of the system, is determined by the eigenvalue equation

$$\mathcal{A}(\psi, \lambda)v = 0, \tag{B2}$$

where ψ serves as a parameter. The eigenvalues of Eq. (B2) depend on ψ and describe continua when ψ is varied.

Equation (9) can be written in the form

$$\frac{\partial}{\partial\psi}\mathcal{A}\frac{\partial\Phi}{\partial\psi} = \mathcal{L}\frac{\partial\Phi}{\partial\psi} + \mathcal{M}\Phi, \tag{B3}$$

where

$$\mathcal{A} = \hat{L}\left(g^{\psi\psi}\hat{L}\Phi\right) + \omega^2 R_0^2 \frac{g^{\psi\psi}}{\bar{v}_A^2 h^4}\Phi, \tag{B4}$$

and the operators $\mathcal{L}$ and $\mathcal{M}$ are certain linear differential operators in angular variables, the exact form of which will not be of importance. The only thing we need to know about them is that $\mathcal{L}$ and $\mathcal{M}$, as well as $\mathcal{A}$, depend linearly on ω^2.

Now we introduce the new (vector) variables

$$v = \frac{\partial\Phi}{\partial\psi}, \quad w = \begin{pmatrix} \Phi \\ \mathcal{A}\frac{\partial\Phi}{\partial\psi} \end{pmatrix}, \tag{B5}$$

and the operators $\mathcal{B}$, $\mathcal{C}$, $\mathcal{D}$ acting on the variables as follows:

$$\mathcal{B}\begin{pmatrix} w_1 \\ w_2 \end{pmatrix} = w_2, \quad \mathcal{C}v = \begin{pmatrix} v \\ \mathcal{L}v \end{pmatrix}, \quad \mathcal{D}\begin{pmatrix} w_1 \\ w_2 \end{pmatrix} = \begin{pmatrix} 0 \\ \mathcal{M}w_2 \end{pmatrix}. \tag{B6}$$

Then Eq. (B3) takes the form of Eq. (B1), where ω^2 plays the part of λ. Hence, the continuous spectrum of Eq. (B3) [and, thus, Eq. (9)] is described by Eq. (B2), which is equivalent to Eq. (60) for the operator $\mathcal{A}$ given by Eq. (B4).

REFERENCES

[1] V. S. Belikov, Ya. I. Kolesnichenko, and V. N. Oraevskij, Zh. Eksp. Teor. Fiz. **55** 2210 (1968); Sov. Phys. JETP **28**, 1172 (1969).

[2] A. B. Mikhailovskij, Zh. Eksp. Teor. Fiz. **68**, 1772 (1975); Sov. Phys. JETP **41**, 890 (1976).

[3] M. N. Rosenbluth and P. Rutherford, Phys. Rev. Lett. **34**, 1428 (1975).

[4] Y. M. Li, S. M. Mahajan, and D. W. Ross, Phys. Fluids **16**, 1466 (1987).

[5] J. Weiland, M. Lisak, and H. Wilhelmsson, Phys. Scr., **T16**, 53 (1987).

[6] C. Z. Cheng and M. S. Chance, Phys. Fluids **29**, 3695 (1986).

[7] J. R. Betti and J. P. Freidberg, Phys. Fluids B **4**, 1465 (1992).

[8] C. E. Kieras and J. A. Tataronis, J. Plasma Phys. **28**, 395 (1982).

[9] R. L. Dewar, R. C. Grimm, J. L. Johnson, E. A. Frieman, J. M. Greene, and P. H. Rutherford, Phys. Fluids **17**, 930 (1974).

[10] M. S. Chu, J. M.Greene, L. L. Lao, A. D. Turnbull, and M. S. Chance, Phys. Fluids B **4**, 3713 (1992).

[11] A. D. Turnbull, E. J. Strait, W. W. Heidbrink *et al.*, Phys. Fluids B **5**, 2546 (1993).

[12] A. Hasegawa and L. Chen, Phys. Rev. Lett. **35**, 370 (1975).

[13] R. R. Mett and S. M. Mahajan, Phys. Fluids B **4**, 2885 (1992).

[14] L. Chen, Phys. Plasmas **1**, 1519 (1994).

[15] C. Z. Cheng, N. N. Gorelenkov, and C. T. Hsu, Nucl. Fusion **35**, 1639 (1995).

[16] C. T. Hsu and D. J. Sigmar, Phys. Fluids B **4**, 1492 (1992).

[17] D. J. Sigmar, C. T. Hsu, R. B. White, and C. Z. Cheng, Phys. Fluids B **4**, 1506 (1992).

[18] K. L. Wong, Plasma Phys. Control. Fusion **41**, R1 (1999).

[19] A. Weller, D. A. Spong, R. Jaenicke *et al.*, Phys. Rev. Lett. **72**, 1220 (1994).

[20] A. Weller and W7-AS team, Survey of MHD Instabilities in W7-AS, Report at 12th International Stellarator Workshop, Madison, USA, September-October 1999.

[21] K. Toi, M. Takechi, S. Ohdachi *et al.*, in *Alpha Particles in Fusion Research, 5th IAEA Technical Committee Meeting, Abingdon, 1997* (Joint European Torus, Abingdon, 1997), p. 197.

[22] N. Nakajima, C. Z. Cheng, and M. Okamoto, Phys. Fluids B **4**, 1115 (1992).

[23] D. A. Spong, B. A. Carreras, C. L. Hedrick, J.-N. Leboeuf, A. Weller, in *Plasma Physics and Controlled Nuclear Fusion Research 1994, 15th IAEA Conference Proceedings, Seville, 1994*, Vol. 3 (IAEA, Vienna, 1996) p. 567.

[24] H. Ninomiya, K. Tobita, U. Schneider, G. Martin, W. W. Heidbrink, and Ya. I. Kolesnichenko, Report on the 6th IAEA Tech. Comm. Mtg on Energetic Particles in Magnetic Confinement Systems, Naka, Japan, 1999, Nucl. Fusion (2000), to be published.

[25] H. Wobig, J. Kisslinger, C. D. Beidler, E. Harmeyer, and F. Herrnegger, Report IAEA-F1-CN-69/FTP/01 in 17th IAEA Conference on Fusion Energy, Yokohama, Japan, 1998, to be published in proceedings of the Conference.

[26] F. Herrnegger, F. Rau, and H. Wobig (editors), Contribution to Wendelstein 7-X and the Helias Reactor 1991-1998, Report IPP 2/343 (Max-Planck-Institut für Plasmaphysik, Garching bei München, 1999).

[27] H. Wobig, Progress in Helias reactor studies, Report IPP III/255 (Max-Planck-Institut für Plasmaphysik, Garching bei München, January 2000).

[28] C. Nührenberg, Phys. Plasmas **6**, 137 (1999).

[29] C. Nührenberg, Plasma Phys. Control. Fusion **41**, 1055 (1999).

[30] G. Grieger, Nucl. Fusion Suppl. **3**, 525 (1991).

[31] F. Wagner, Transactions of Fusion Technology **33**, 67 (1998).

[32] C. Schwab, Phys. Fluids B **5**, 3195 (1993).

[33] *Wendelstein VII-X. Application for preferential support* (Wendelstein Project Group, August 1990).

[34] A. H. Boozer, Phys. Fluids **24**, 1999 (1981).

[35] R. B. White and M. S. Chance, Phys. Fluids **27**, 2455 (1984).

[36] E. Strumberger, First survey of finite-beta magnetic field of W7-X, Report IPP2/339, (Max-Planck-Institut für Plasmaphysik, Garching bei München, December 1997).

[37] E. Strumberger, H. Wobig, J. Kisslinger, and C. Nührenberg, Equilibrium and Stability Properties of a Helias Reactor, Report IPP III/249 (Max-Planck-Institut für Plasmaphysik, Garching bei München, 1999).

[38] J. W. Van Dam, G.-Y. Fu, and C. Z. Cheng, Fusion Technol. **18**, 461 (1990).

[39] G. Y. Fu, Phys. Plasmas **2**, 1029 (1995).

[40] H. L. Berk, J. W. Van Dam, D. Borba, *et al.*, Phys. Plasmas **2**, 3401 (1995).

[41] S. M. Mahajan, D. W. Ross, and G.-L. Chen, Phys. Fluids **26**, 2195 (1983).

[42] H. L. Berk, J. W. Van Dam, Z. Guo, and D. M. Lindberg, Phys. Fluids B **4**, 1806 (1992).

[43] D. A. Garren and A. H. Boozer, Phys. Fluids B **3**, 2805 (1991).

[44] B. A. Dubrovin, S. P. Novikov, and A. T. Fomenko, *Sovremennaya geometriya* (Moscow, Nauka, 1979) [in Russian].

[45] E. Hameiri, Phys. Fluids **24**, 562 (1981).

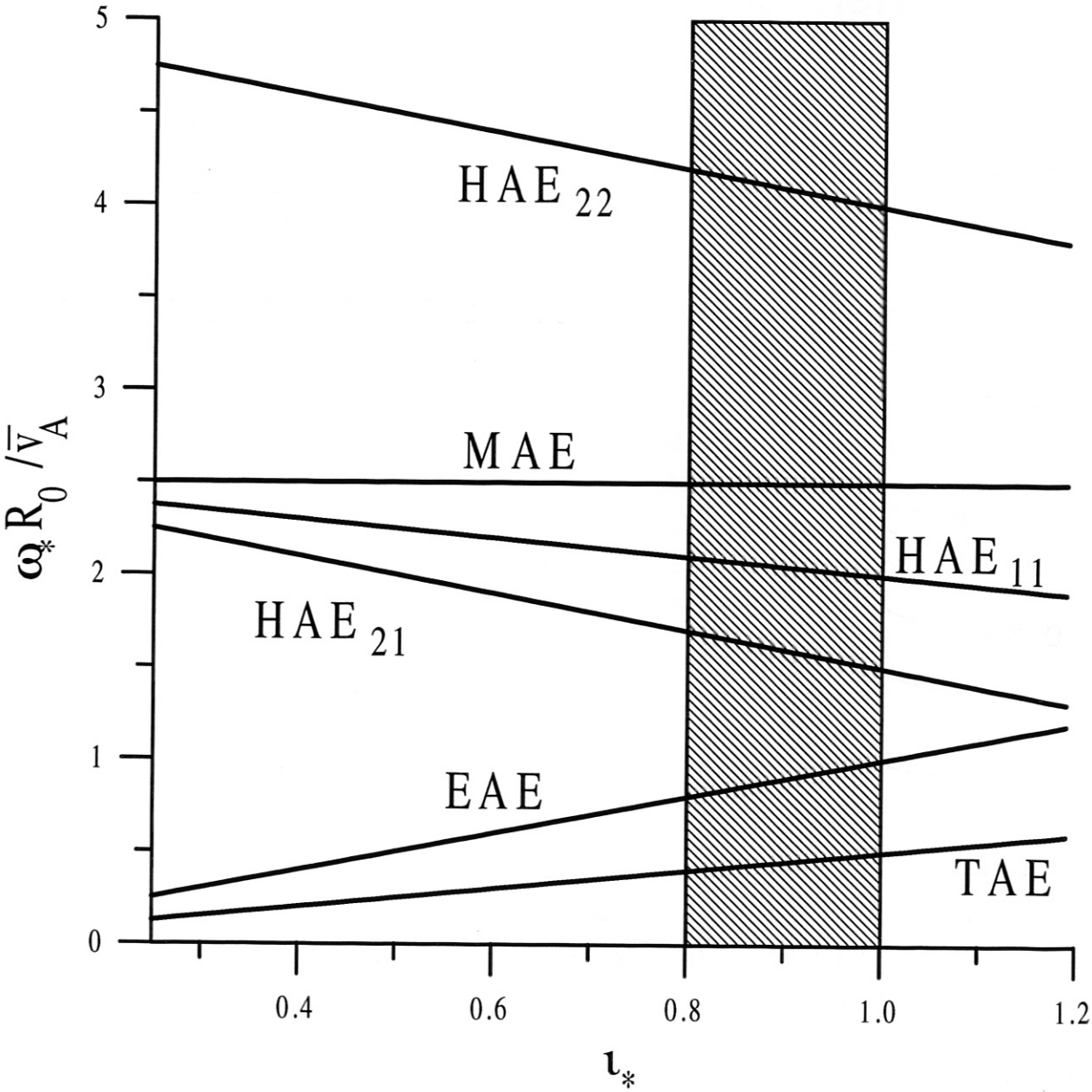

FIG. 1. Characteristic frequencies of various kinds of AEs according to Eqs. (30)–(32), (39)–(41). The hatched region corresponds to a Helias reactor.

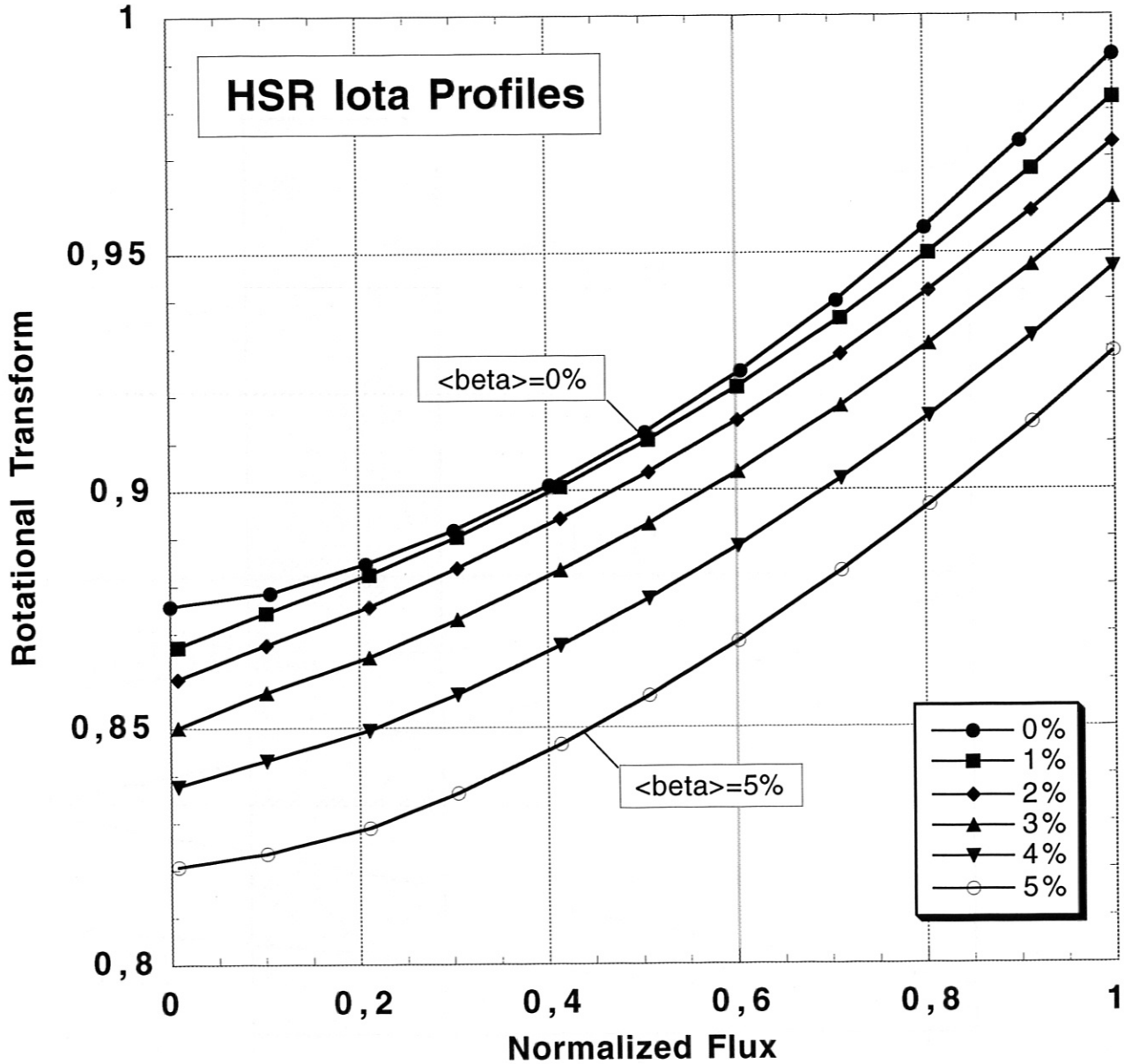

FIG. 2. Radial dependence of the rotational transform for various β in a Helias reactor [37].

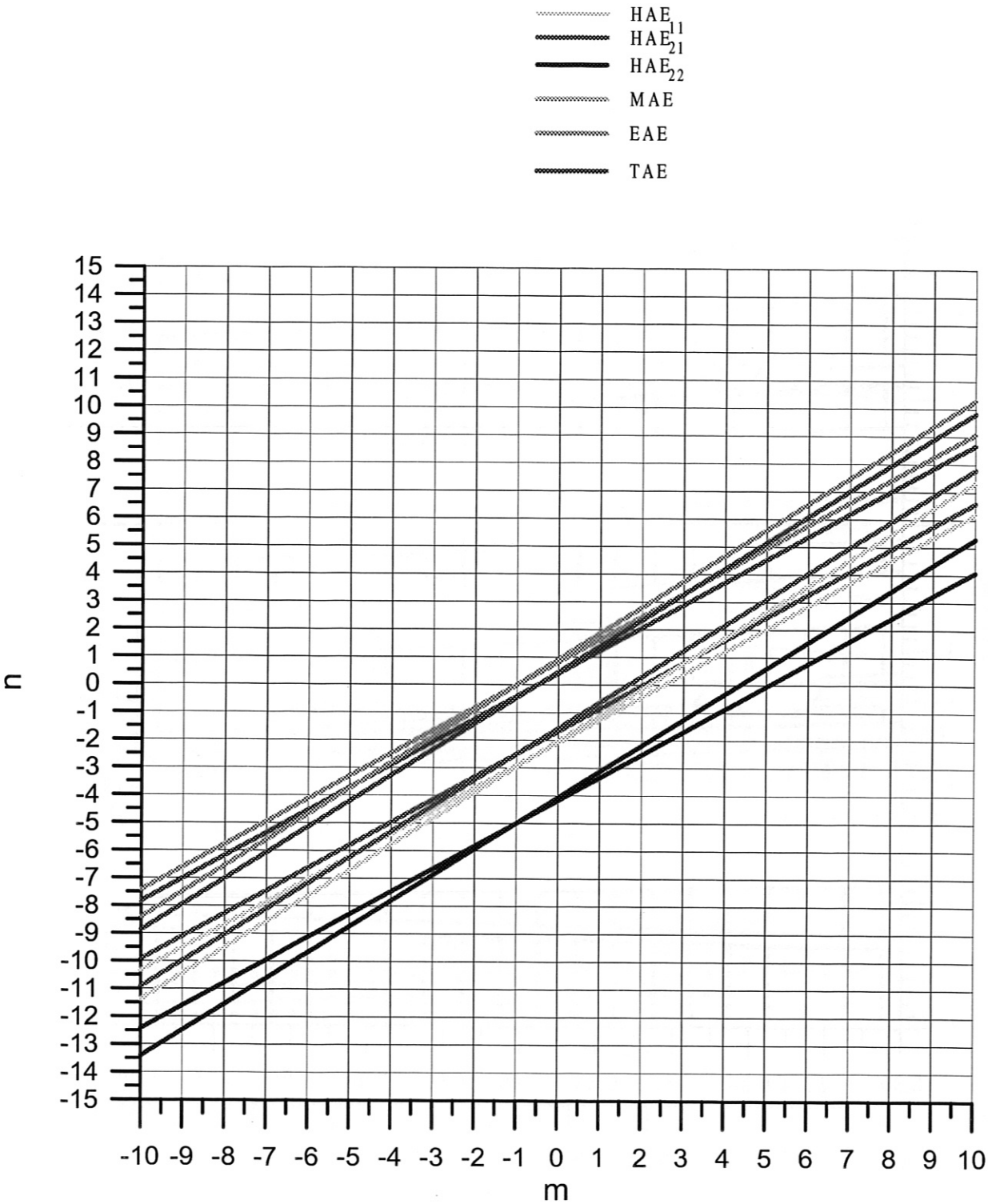

FIG. 3. Dependence of n on m determined by Eqs. (30)–(32), (39)–(41) for $\iota_* = \iota(0)$ and $\iota_* = \iota(a)$ in a Helias reactor with $\beta = 4.7\%$ [37]. The integer points within each corridor correspond to the mode numbers of the waves involved in the corresponding type of coupling.

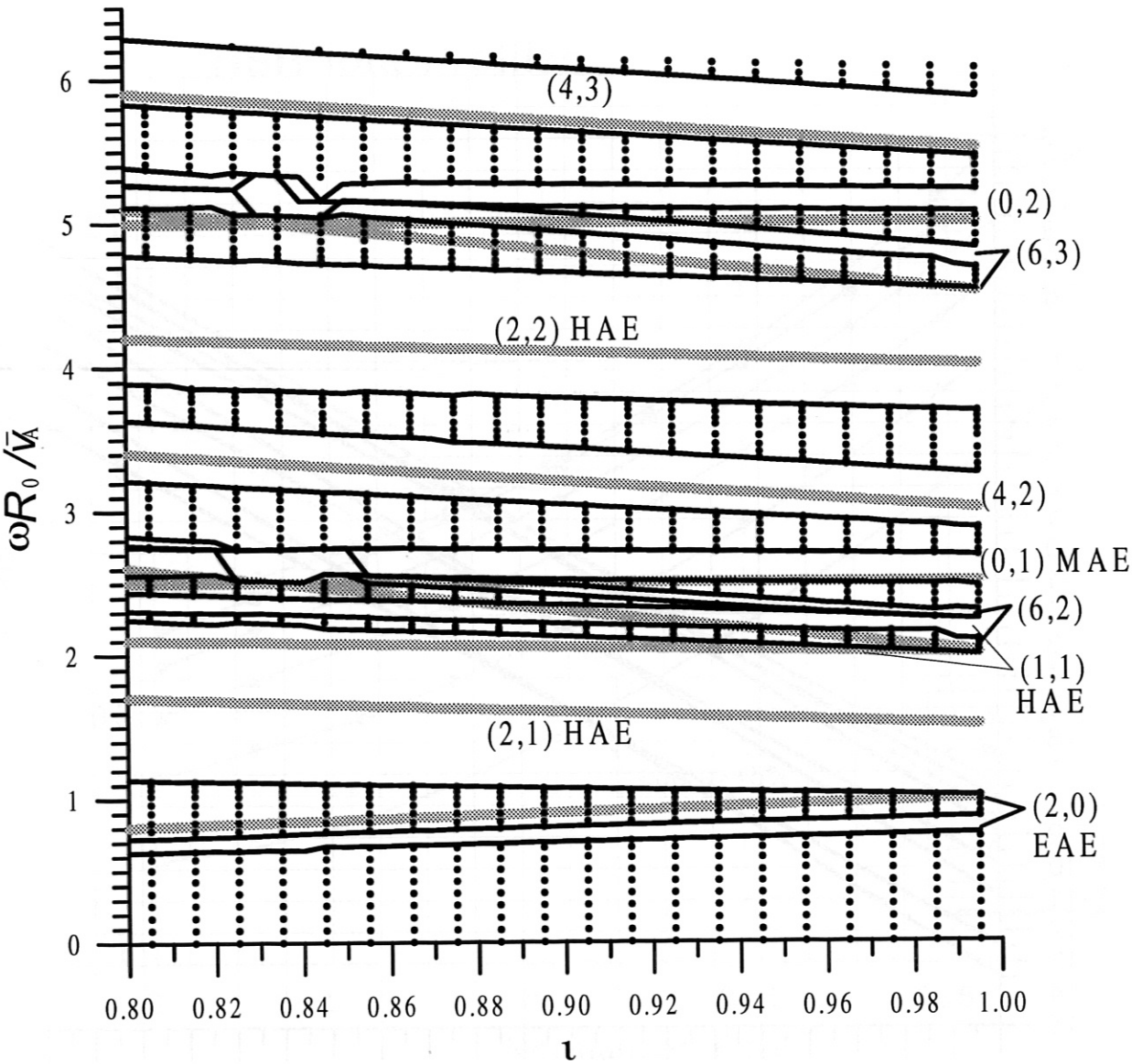

FIG. 4. Gaps in the Alfvén continuum. The gaps are labeled by the coupling numbers (μ, ν) responsible for the formation of each gap. Dots, the calculated frequencies of the continuum spectra obtained as $\tilde{k}$ of the dominant harmonic was scanned; thin lines, the calculated "banks" of the gaps for various coupling numbers (μ, ν); wide grey lines, the places where the same gaps would be located for the infinitely small coupling parameters ϵ_g, ϵ_c (cf. Fig. 1).

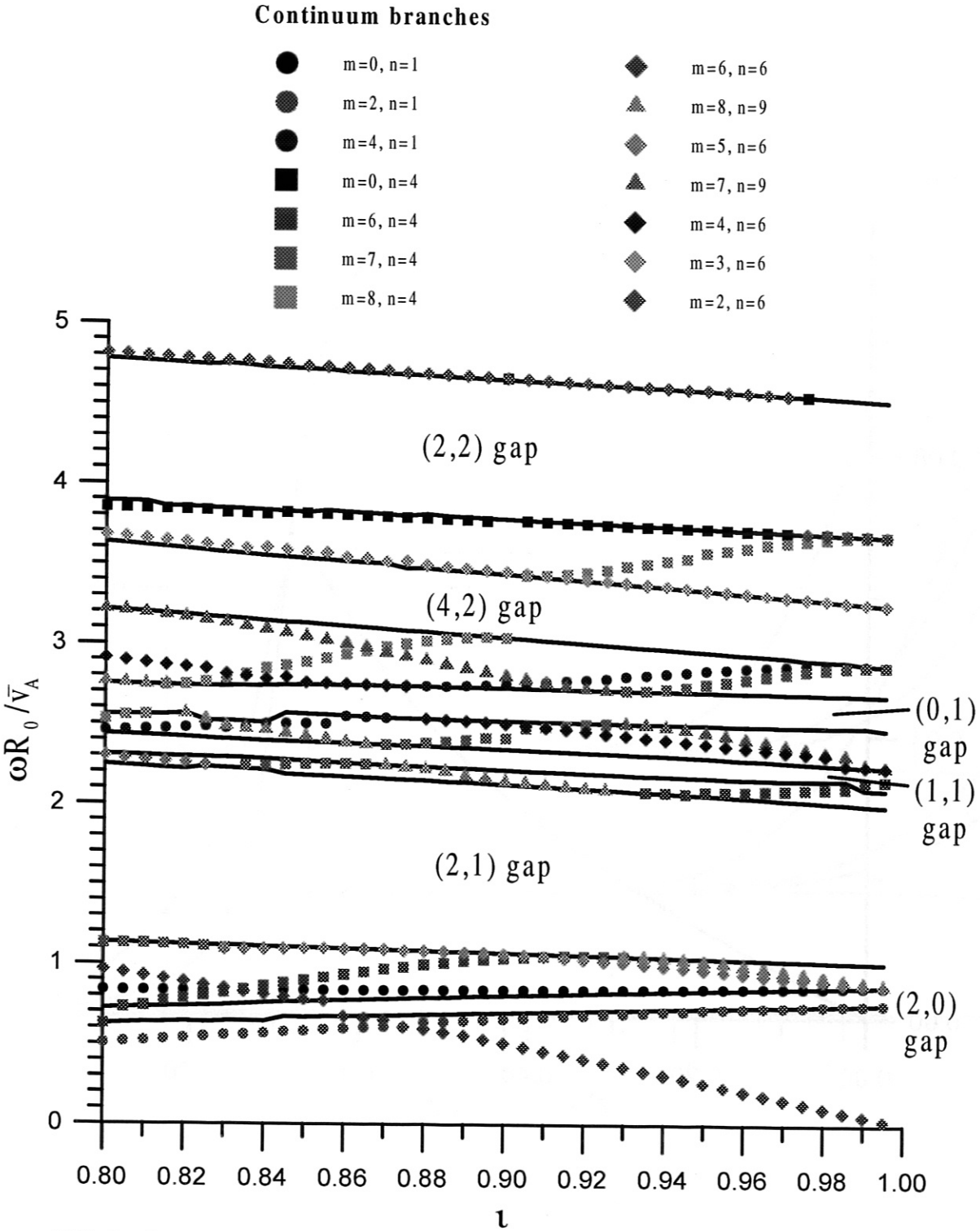

FIG. 5. Continuum branches with certain selected mode numbers m and n. Solid lines, the calculated "banks" of the most important gaps, which are labeled by the associated coupling numbers (μ, ν).

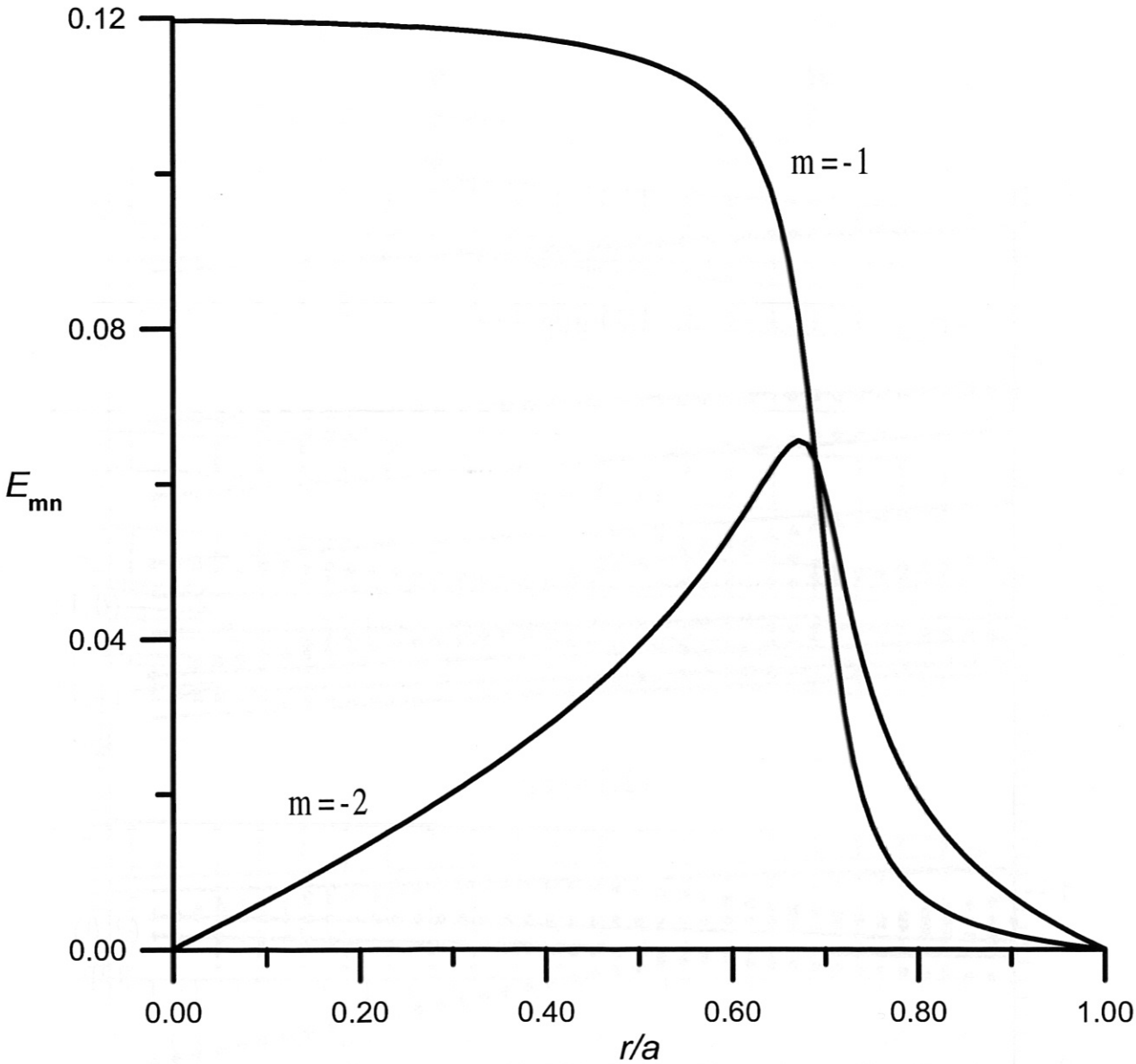

FIG. 6. The test calculation of the TAE structure for the mode with $n = -1$ in a homogeneous tokamak plasma with $q(r) = 1 + r^2/a^2$. This picture coincides with the result of Ref. [38].

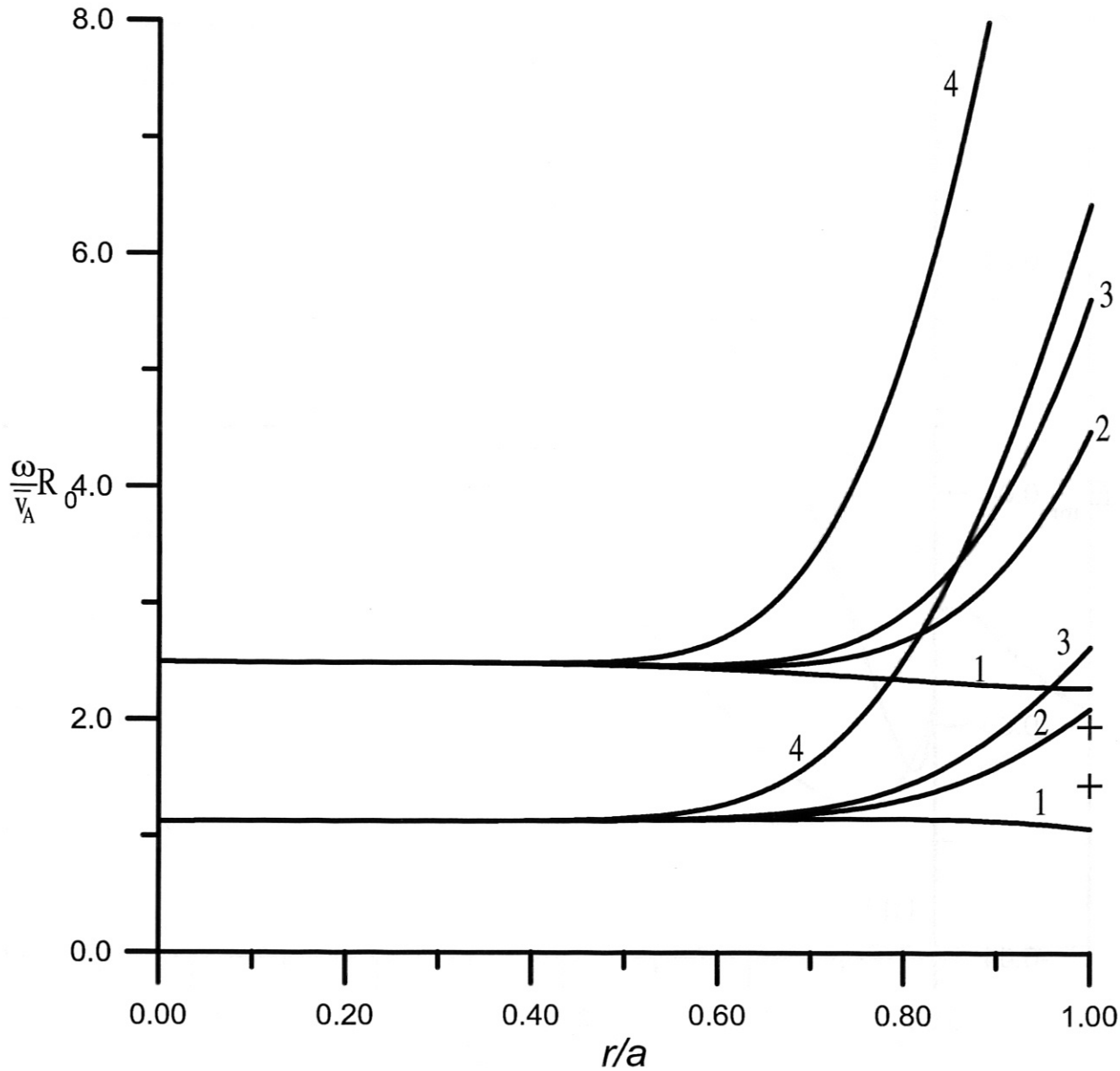

FIG. 7. The HAE_{21} gap for the coupled $m = 3$, $n = 1$ and $m = 5$, $n = 6$ modes in homogeneous and inhomogeneous plasmas. 1, $n(r) = \text{const}$; 2, $x_n = 0.9$; 3, $x_n = 0.85$, 4, $x_n = 0.7$; x_n is a parameter in $\rho(r) = \rho(0)[1 + r/(x_n a)]^{-1}$. Crosses show the eigenfrequencies in the homogeneous plasma, $\lambda_1 = 1.4406$ and $\lambda_2 = 1.9464$, normalized to $\bar{v}_A/R_0$.

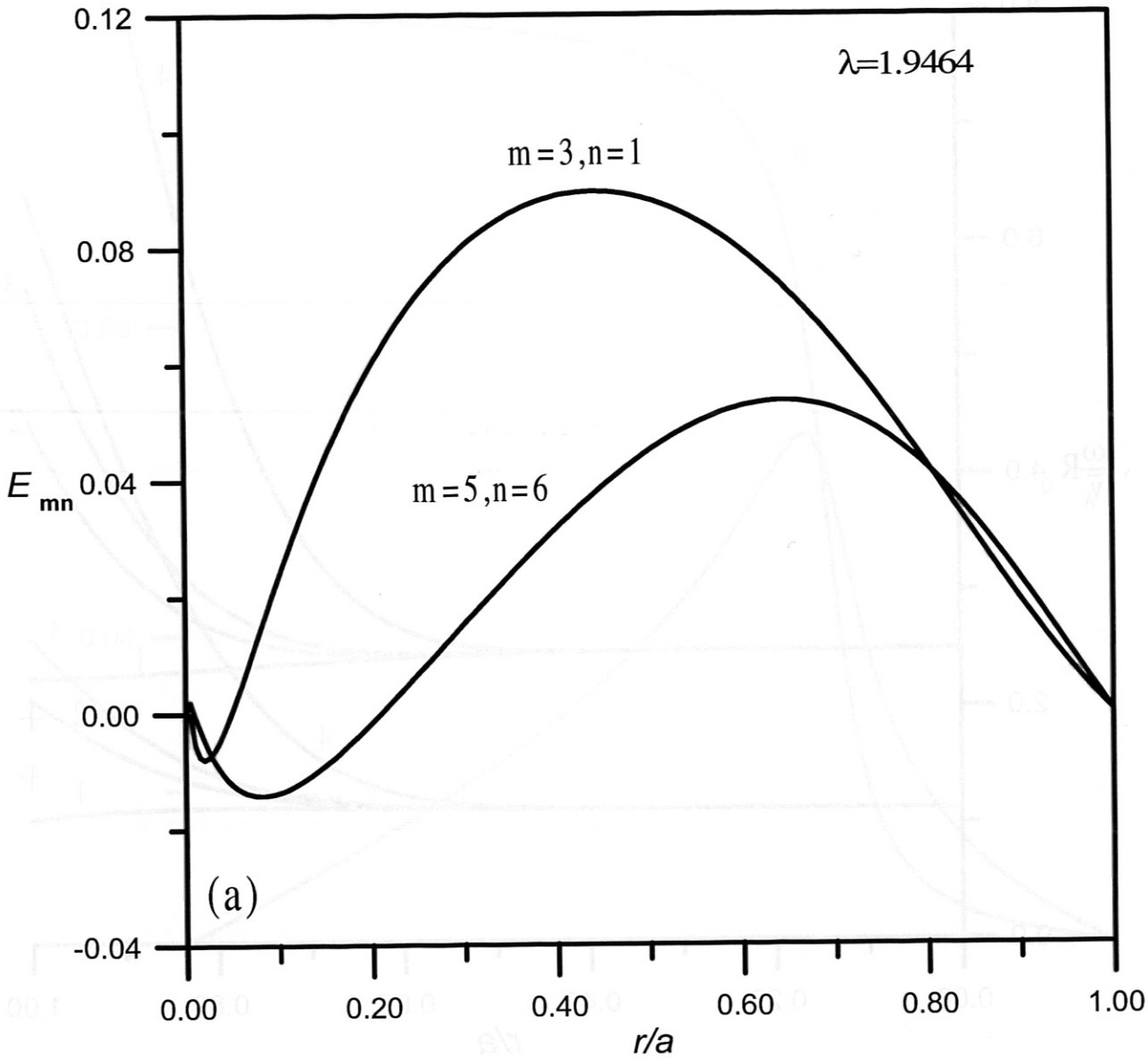
0.12
0.08
0.04
0.00
-0.04
E_{mn}
λ=1.9464
m=3,n=1
m=5,n=6
(a)
0.00
0.20
0.40
0.60
0.80
1.00
r/a

FIG. 8.

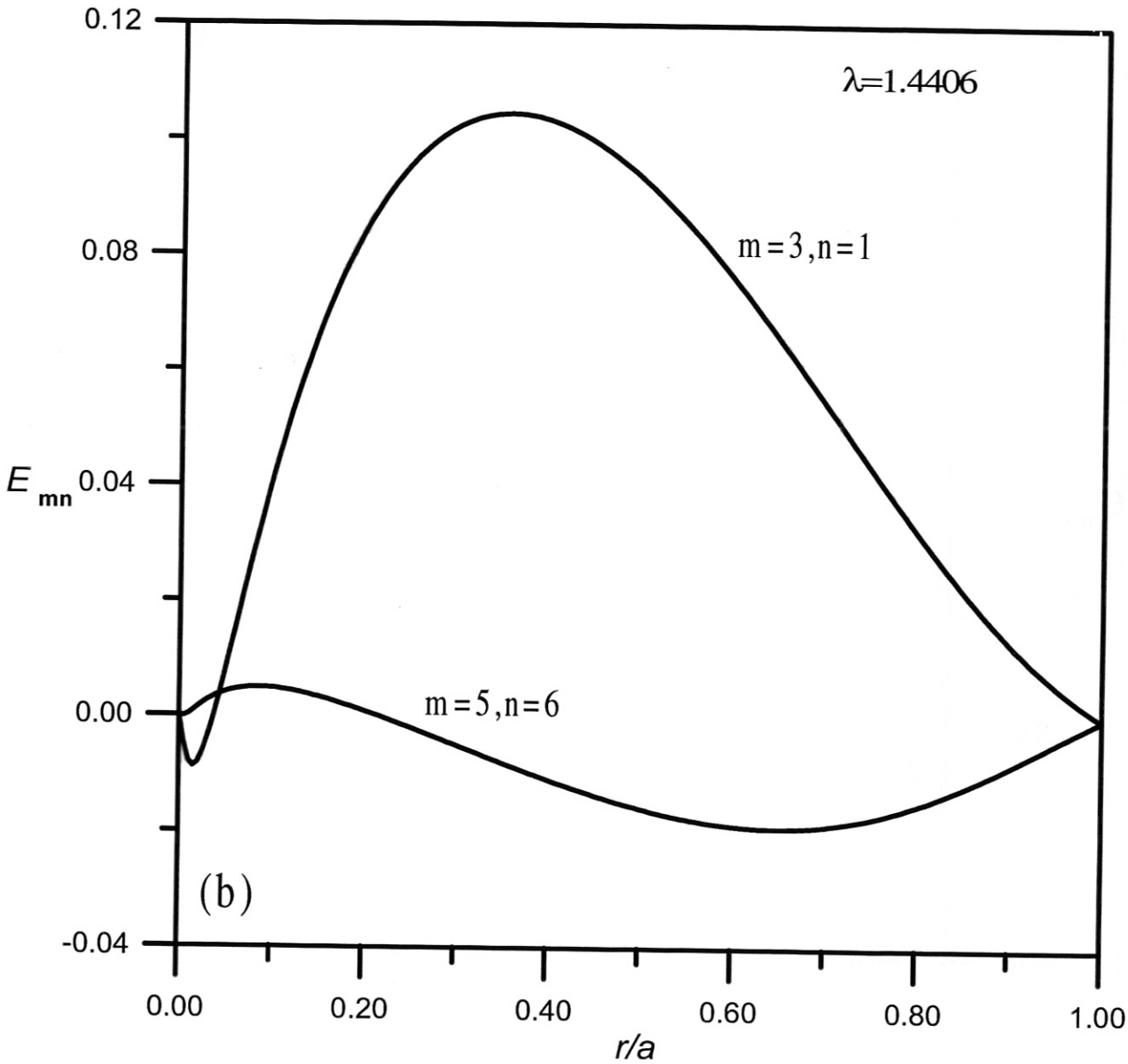

FIG. 8. The radial structure of the HAE_{21} mode with the same mode numbers as in Fig. 7 in the homogeneous plasma. (a) $\lambda = 1.9464$; (b) $\lambda = 1.4406$.

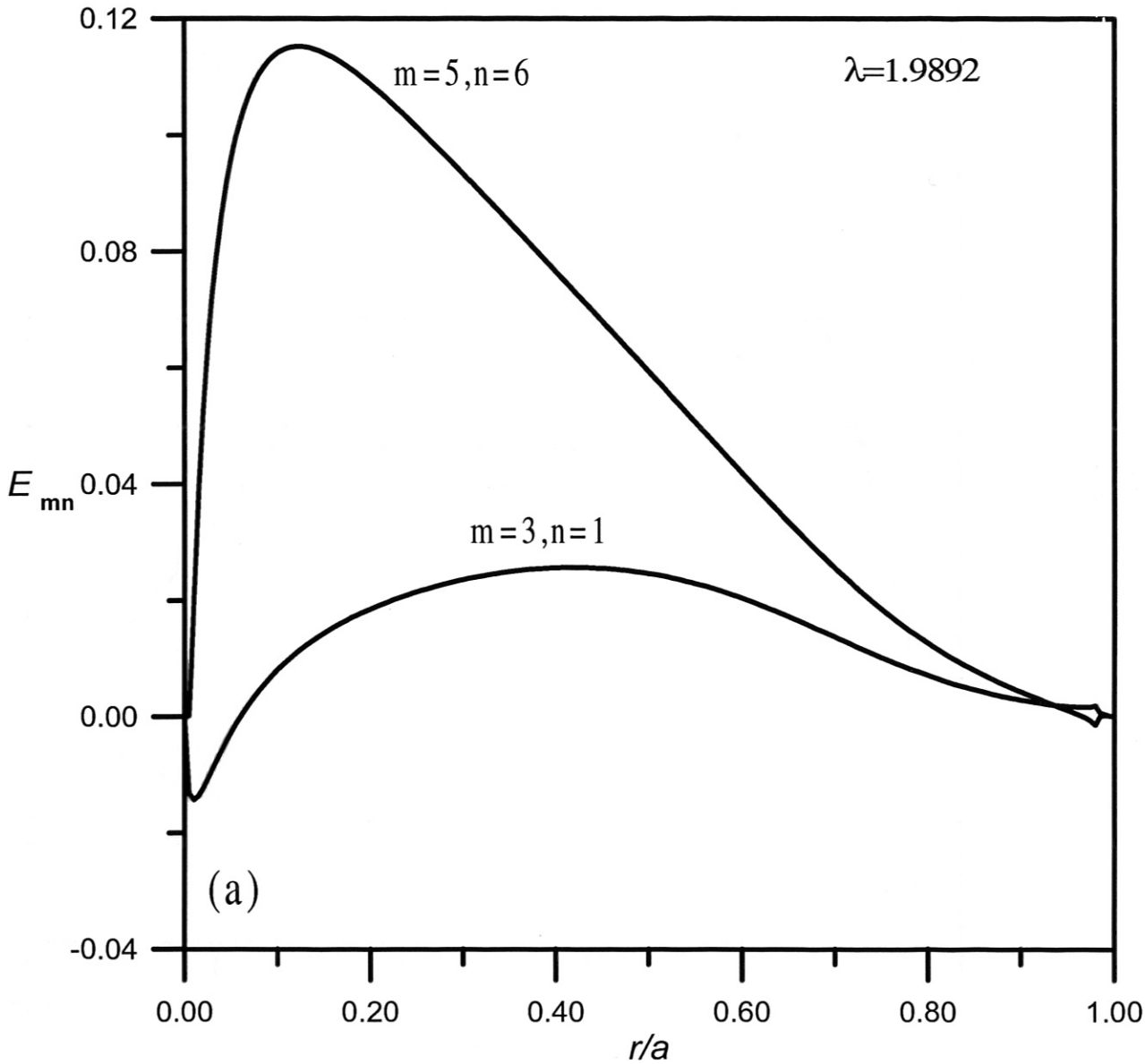
0.12
0.08
0.04
0.00
-0.04
E_{mn}
m=5,n=6
λ=1.9892
m=3,n=1
(a)
0.00
0.20
0.40
0.60
0.80
1.00
r/a

FIG. 9.

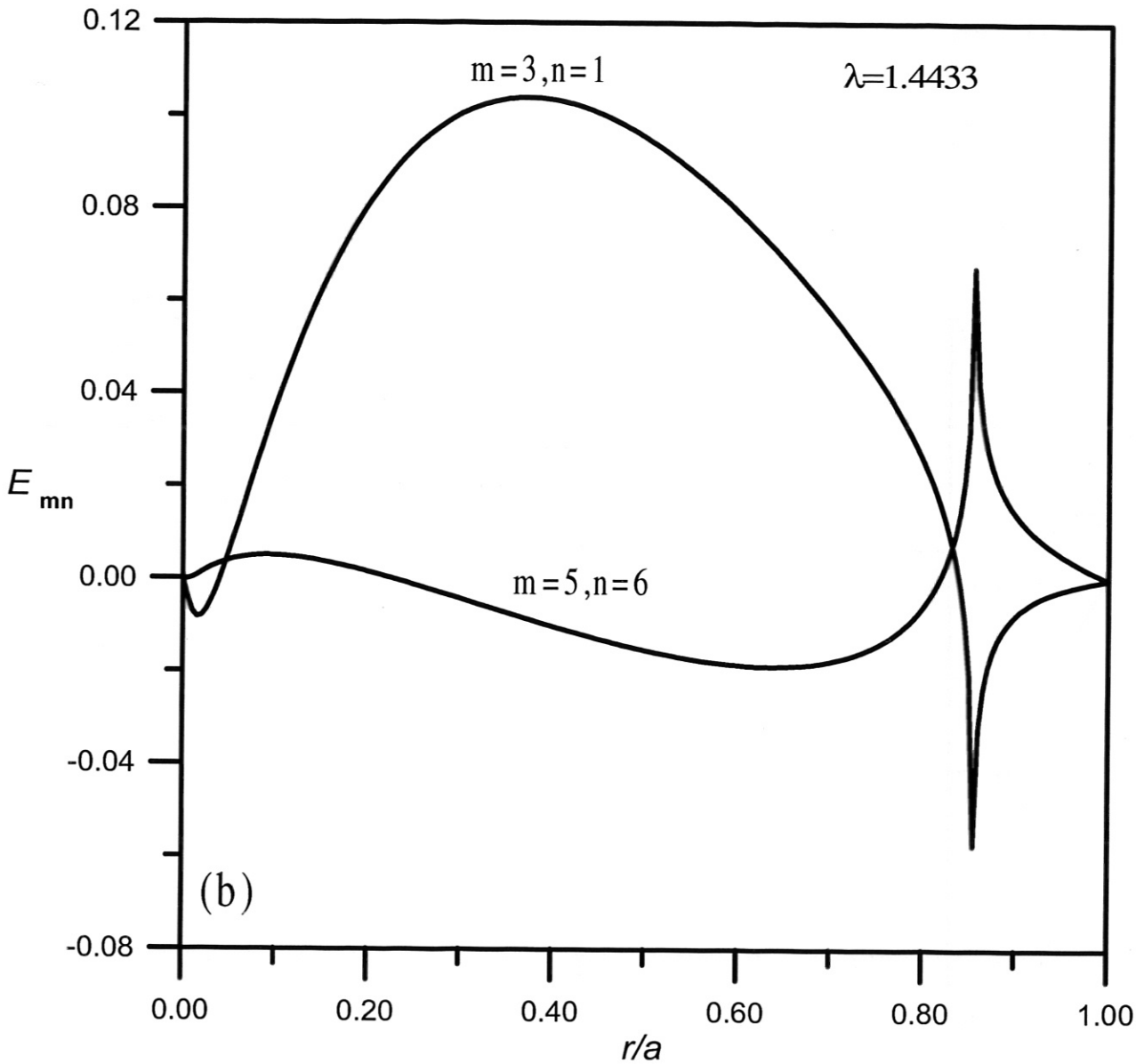

FIG. 9. The radial structure of the HAE_{21} mode with the with the same mode numbers as in Fig. 7 in the inhomogeneous plasma with $x_n = 0.9$; (a) $\lambda = 1.9892$, (b) $\lambda = 1.4433$. The spikes near the plasma edge indicate that the modes with higher and lower λ undergo weak and strong continuum damping, respectively.

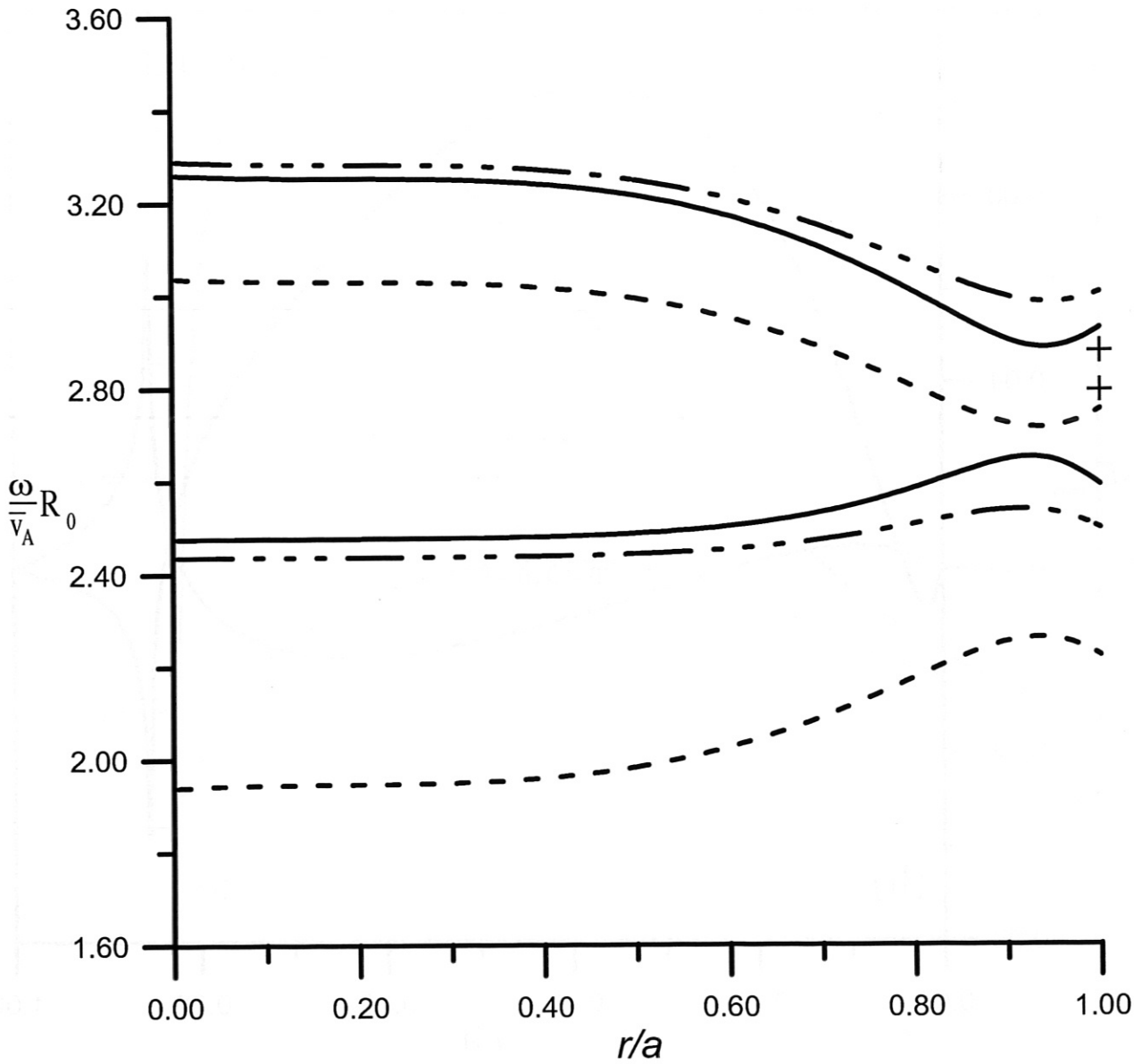

FIG. 10. MAE gap associated with the intersection of the cylindrical Alfvén continua with $m = 4$, $n = 1$ and $m = 4$, $n = 6$ in the homogeneous plasma. Solid line, the effect of the coupling parameters $\epsilon^{(01)}$, $\epsilon^{(21)}$ and $\epsilon^{(20)}$ is taken into account; dot-dashed line, the effect of coupling parameters $\epsilon^{(21)}$ and $\epsilon^{(20)}$ is taken into account; dashed line, two-mode approximation with $\epsilon^{(01)} \neq 0$. Crosses show two eigenfrequencies in the solid-line gap.

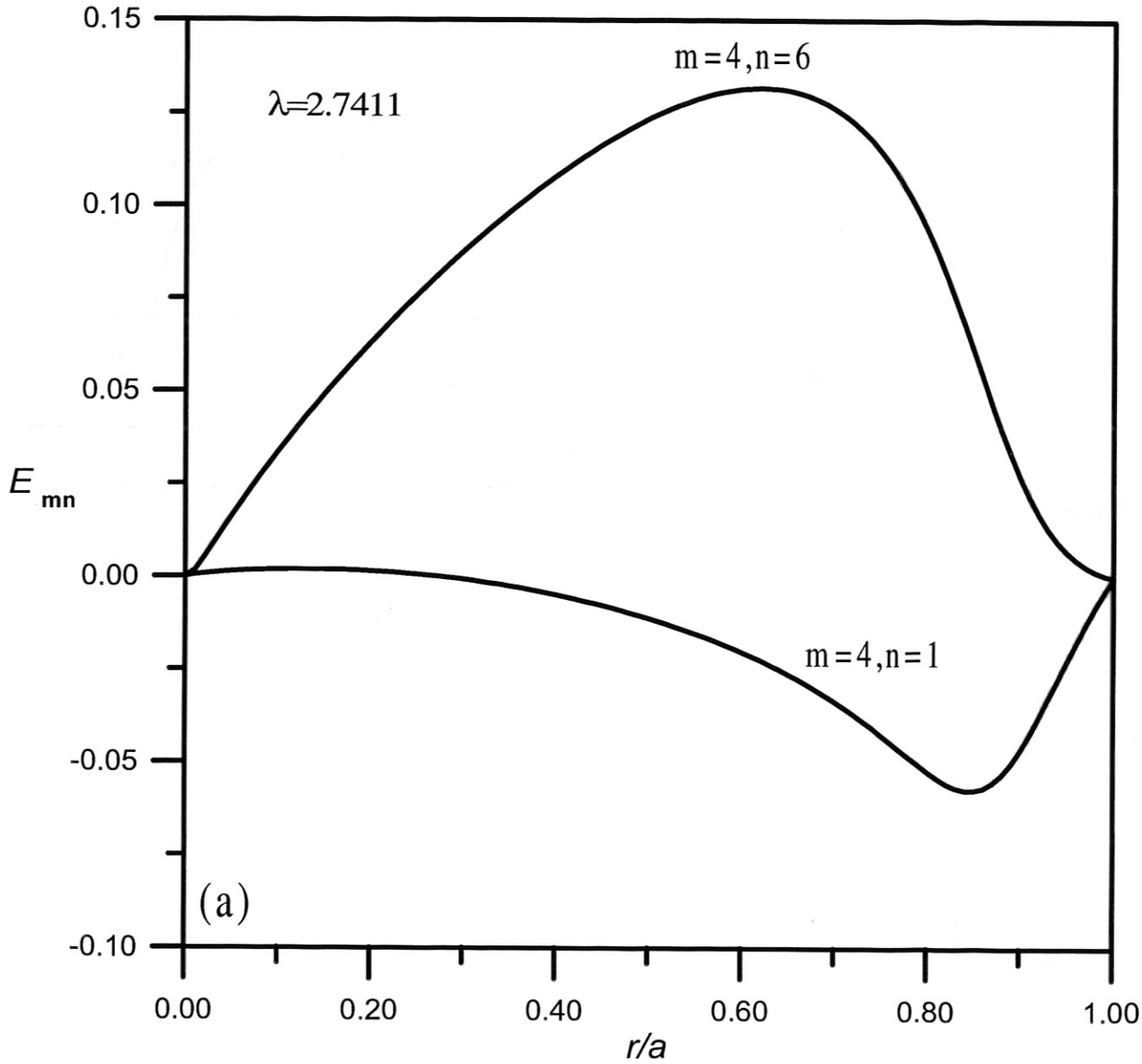
0.15
0.10
0.05
0.00
-0.05
-0.10
E_{mn}
m=4,n=6
λ=2.7411
m=4,n=1
(a)
0.00
0.20
0.40
0.60
0.80
1.00
r/a

FIG. 11.

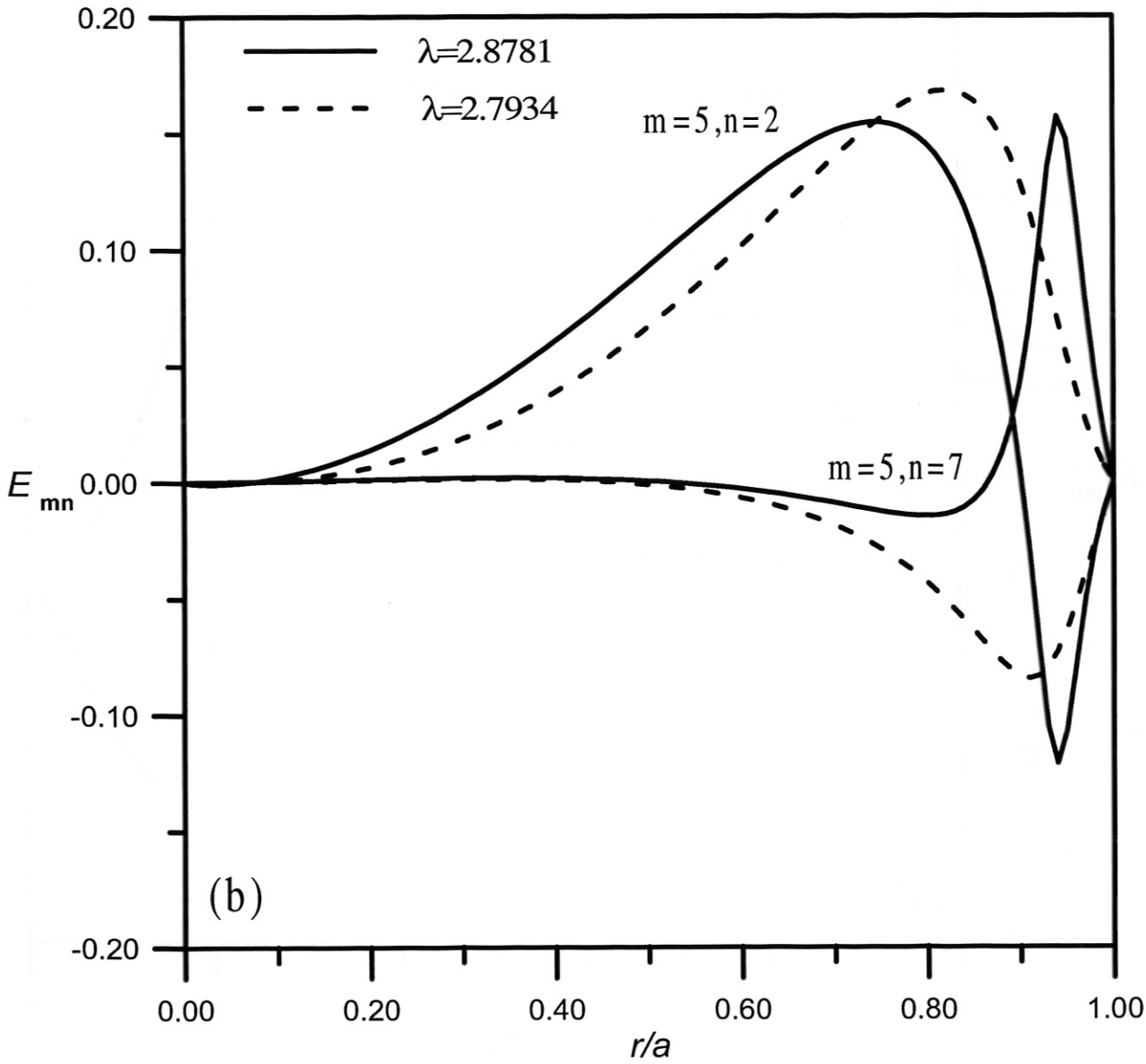

FIG. 11. Radial structure of MAE modes. (a) $m = 4$, $n = 1$ and $m = 4$, $n = 6$; (b) $m = 5$, $n = 2$ and $m = 5$, $n = 7$.

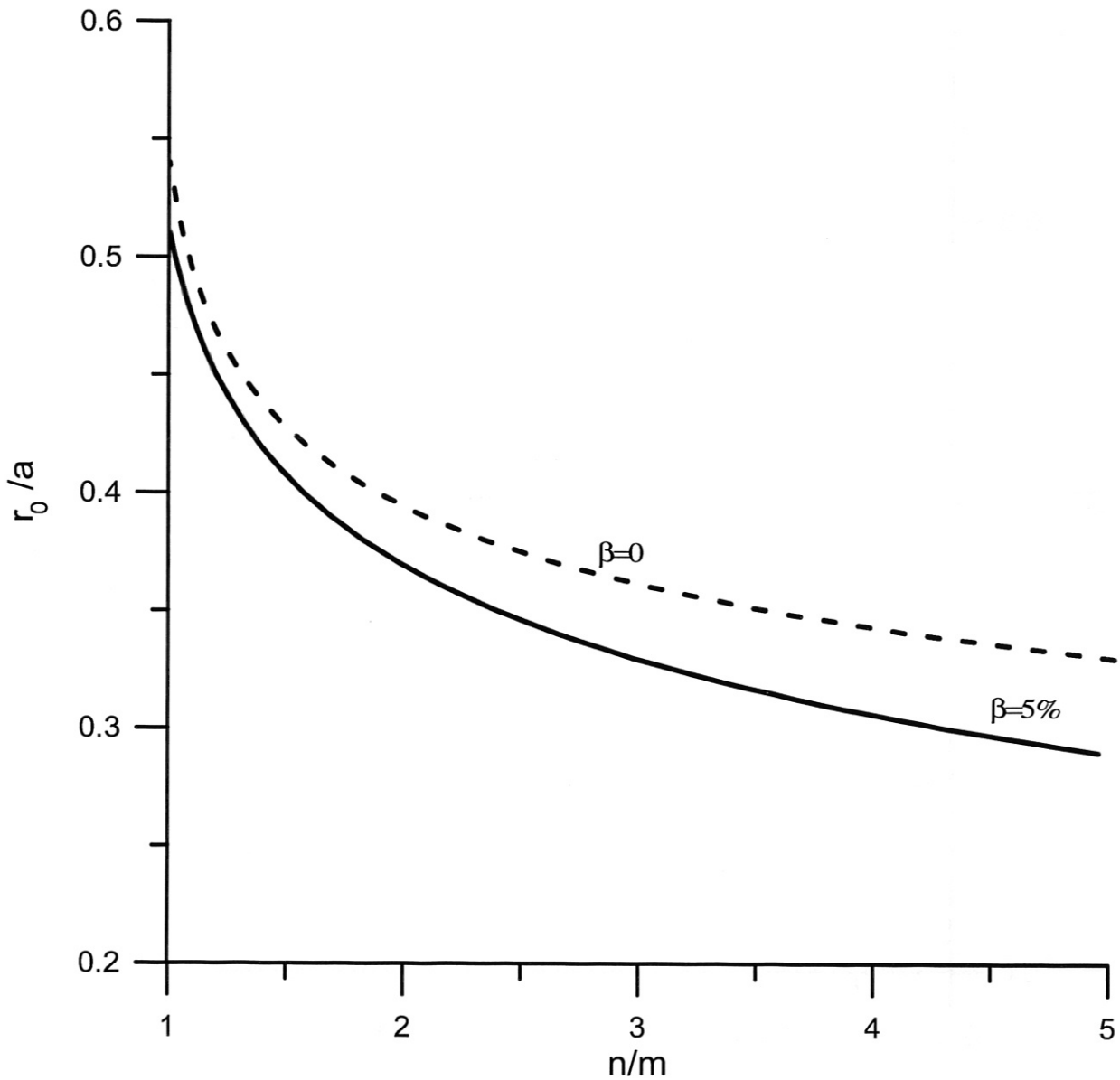

FIG. 12. Location of minimum of the local Alfvén frequency versus n/m in a Helias reactor with the inhomogeneity parameter $x_n = 0.7$.

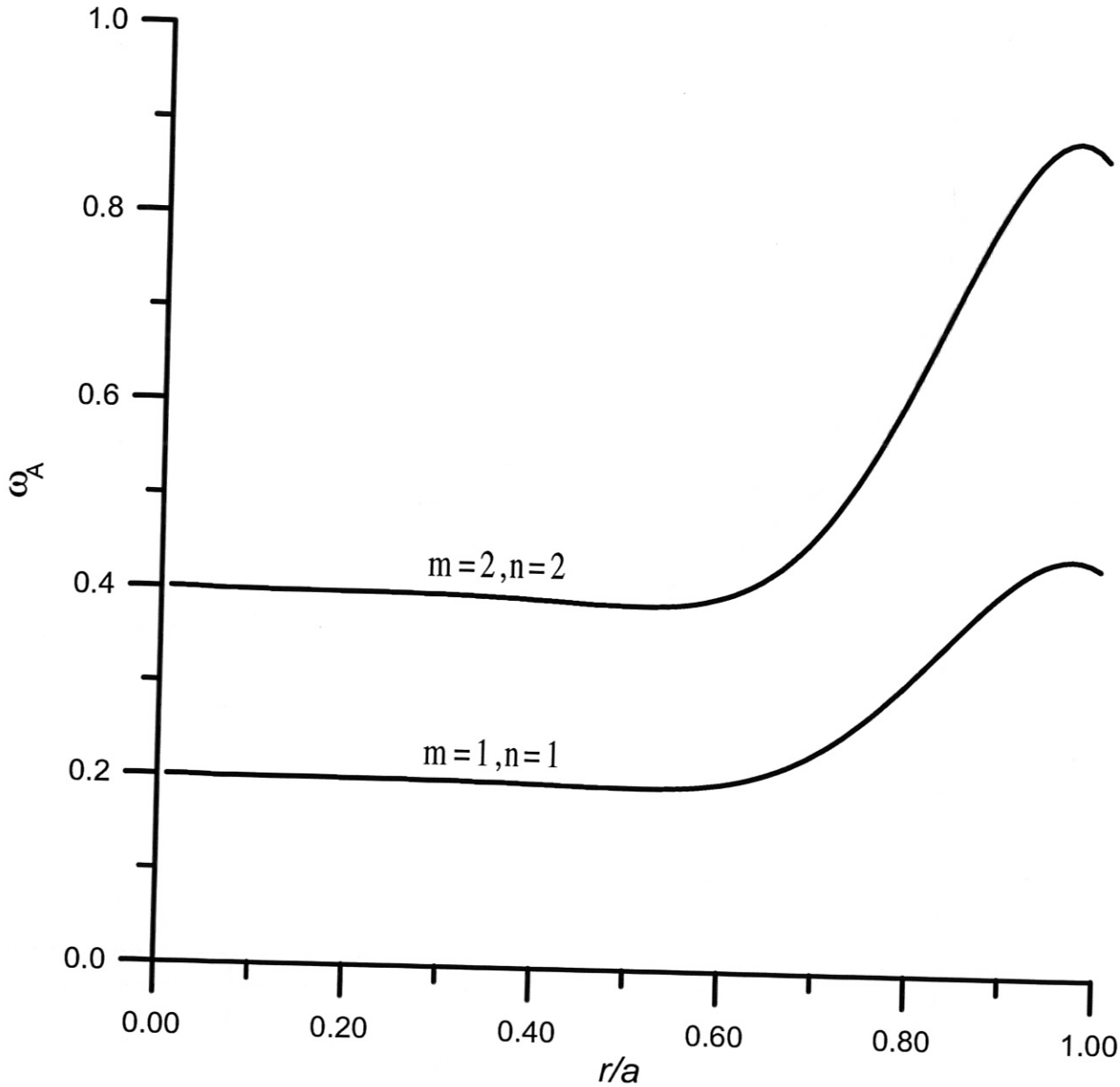

FIG. 13. Cylindrical Alfvén continua for the same inhomogeneity parameter as in Fig. 12 and $\beta = 5\%$.

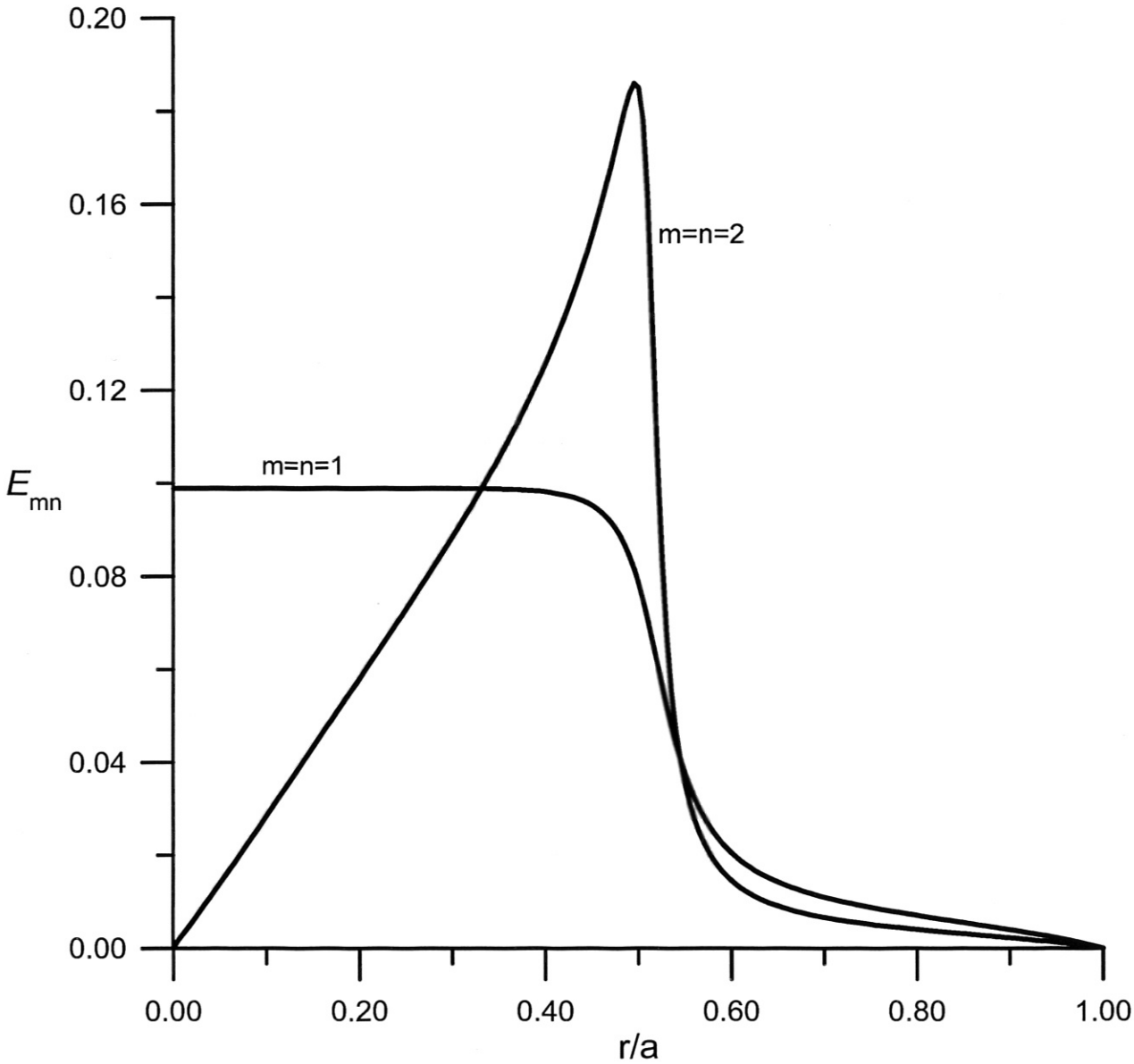

FIG. 14. Radial structure of GAE modes in a plasma with the same parameter as in Fig. 12 and $\beta = 5\%$.